

Adaptive fast nonsingular terminal sliding mode tracking control for quadrotor with disturbances compensation and actuator saturation

Proc IMechE Part C:
J Mechanical Engineering Science

I–19

© IMechE 2023

Article reuse guidelines:

sagepub.com/journals-permissions

DOI: 10.1177/09544062231167026

journals.sagepub.com/home/pic



Hujie Wei and Yan Jiang 

Abstract

This paper designs the double closed-loop control system combining nonlinear disturbances observers (NDOB) and an adaptive fast nonsingular terminal sliding mode (AFNTSM) for the tracking control problem of quadrotor under external disturbances, actuator saturation and unmodeled dynamics. The NDOB-AFNTSM method avoids the singularity problem. To compensate for disturbances, an adaptive strategy estimates the unknown bound of NDOB errors and the unknown bound of disturbances. Besides, new fast reaching law shortens convergence times. The dead zone method is chosen to avoid over-estimation and system divergence. Considering actuator saturation, this paper uses an anti-saturation auxiliary compensator to compensate for unknown saturation errors. System stability is confirmed by the Lyapunov direct method. The simulation results reveal that the proposed method improves convergence speed and accuracy, which is more robust than similar methods. Finally, two comparative studies for performance indexes in simulation demonstrate the preferable performance of the proposed method.

Keywords

Quadrotor, NDOB-AFNTSM, chattering, tracking control, actuator saturation, performance indexes

Date received: 10 August 2022; accepted: 6 February 2023

Introduction

Since the 21st century, research in Unmanned Aerial Vehicle (UAV) has attracted numerous scholars. The UAV is deployed in the military field and civilian field including undertaking rescues and power inspection.^{1,2} The quadrotor is a kind of UAV which owns highly flexible maneuverability. Due to the highly coupled, underactuated, and nonlinear features of the quadrotor,³ the outstanding controller becomes the assurance of quadrotors to achieve precise tracking.

Some scholars initially adopted conventional linear schemes for flight control of quadrotor such as PID method,⁴ LQR scheme.⁵ However, the external disturbance, parameter uncertainty and actuator failure damage the control performance and even destroy the tracking effect. To improve the robustness, more developed nonlinear methods and intelligent control methods were subsequently applied for quadrotor tracking such as backstepping method,^{6,7} ADRC approach,⁸ feedback linearization method,⁹ neural network scheme,¹⁰ sliding mode control (SMC) approach.^{11,12} One of the superior methods for quadrotor is the SMC because of its properties such as insensitivity to external disturbances and high

accuracy.¹³ Terminal sliding mode control (TSMC) is proposed by Yu et al.,¹⁴ which not only preserves the advantages of SMC, but also enables the errors to reach zero in a limited time. Although the TSMC shortens the convergence time, the TSMC has singularities, which is not allowed by the computer. Nonsingular TSMC is used by Feng et al.,¹⁵ which solves the singularity problem.

Considering the low performance of single algorithm, compound algorithms is the mainstream. Some representative works of SMC method applied to quadrotor have achieved important advances, for examples: a modified super-twisting SMC method is presented with reduced control effort and accurate tracking, and overcame the drawback of classical super-twisting.¹⁶ Razmi and Afshinfar¹⁷ combined neural network adaptive scheme with SMC method, and obtained a tiny overshoot and a settling time.

School of Electrical Engineering, Guangxi University, Nanning, China

Corresponding author:

Yan Jiang, School of Electrical Engineering, Guangxi University, No.100, Daxuedong Road, Xixiangtang District, Nanning 530004, China.
Email: yanjiang986@126.com

Some works used compound fractional-order sliding manifold with a new degree of freedom; the merit of this method is that fractional term can weaken the chattering effect and is suitable for integer order systems.^{18,19} Wang et al.²⁰ gave an adaptive event-triggered SMC scheme with asymmetric output constraints which solves the “explosion of complexity” problem. Mechali et al.²¹ proposed a continuous SMC method which ensures that sliding motion is fixed-time stable independently of initial condition, and the authors set a model-based design framework to conduct the control algorithms in real autopilot hardware. An adaptive fractional-order SMC method is designed for quadrotors leader-follower formation control.²² Zhao et al.²³ designed an integral sliding mode controller for quadrotor with a nonlinear extended observer and verified the efficient wind resistance by outdoor flight.

Driven by the above discussion, an NDOB-AFNTSM scheme is proposed in this paper to tackle the tracking control problem of the quadrotor subjected to partially unmodeled dynamics, actuator saturation and complex external disturbances. The NDOB compensates for the external disturbances of the position subsystem. The merit of NDOB-AFNTSM strategy is that the adaptive laws effectively estimate the upper bound of the unknown disturbances and the upper bound of NDOB errors. Besides, the position subsystem adopts a new reaching law which guarantees that the velocity near the sliding mode surface is as small as possible. Further, the control inputs of a quadrotor are bounded in the real environment, and many studies have ignored this issue. In this paper, we adopt an anti-saturation auxiliary compensator to compensate unknown saturated errors to handle this problem. The simulation results confirm that the quadrotor can maintain good tracking with small controller chattering and good performance indexes compared with similar methods.^{24–26}

The main contributions of this paper are highlighted as follows:

- (i) Distinct from some works^{27,28} which also used NTSMC, this paper takes full account of the boundedness of the actuator input in practical applications and uses an anti-saturation auxiliary compensator to effectively solve the actuator saturation problem. This compensator do not require a priori information about the saturation errors and is simple to adjust the parameter, thus offsetting the effect of the actual saturation error and ensuring that the system consumes less energy by suppressing unreasonably high gain inputs based on the bounded ideal control inputs.
- (ii) Compared with the existing scheme of TSMC combined with nonlinear disturbances observers,^{29,30} this paper employs not only the observer to compensate for disturbances, but also the

adaptive method to compensate for the unknown upper bound of the observer error. The robustness to unmodeled dynamics and external disturbances of the system is further enhanced and the chattering caused by switching control gains is further attenuated.

- (iii) The new reaching law in NDOB-AFNTSM method effectively guarantees the fast rapidity of the sliding mode reaching phase and suppresses chattering compared with works.^{25,26} Unlike work from Labbadi and Cherkaoui,²⁷ this paper utilizes the dead zone method to prevent over-estimation. The NDOB-AFNTSM avoids singularity of the existing TSMC and ensure fast convergence for errors. The quantitative analysis of performance index is given to determine the superiority of this scheme over NTSMC on control precision and anti-chattering ability.

The rest of this article contains the following sections. The quadrotor dynamics model is provided in section “Problem formulation.” Section “Controller design” describes the proposed NDOB-AFNTSM strategy. The simulation results and comparison with similar methods are presented in Section “Simulation results.” Section “Conclusion” makes a summary.

Problem formulation

The quadrotor used in this paper is a cross-type quadrotor. The schematic diagram of the quadrotor is shown in Figure 1. Four motors is distributed with different rotational speeds to generate forces on three axes, thus the quadrotor is driven to move and rotate. Some assumptions are given as follows:

Assumption 1. Quadrotors are homogeneous rigid bodies.

Assumption 2. The quadrotor flies in a steady environment.

Define the earth-frame as $\mathbf{E} = (o_e, x_e, y_e, z_e)$ and define the body-frame as $\mathbf{B} = (o_b, x_b, y_b, z_b)$. The quadrotor position and attitude are indicated by $\xi = [x, y, z]^T$ and $\zeta = [\phi, \theta, \psi]^T$, $\phi \in (-\frac{\pi}{2}, \frac{\pi}{2})$, $\theta \in (-\frac{\pi}{2}, \frac{\pi}{2})$, $\psi \in (-\pi, \pi)$, separately. The attitude angles are roll, pitch and yaw respectively. Vector conversion from \mathbf{B} to \mathbf{E} is expressed by rotation matrix C_B^E :

$$\begin{bmatrix} c\theta c\phi & s\theta c\phi s\psi - c\psi s\phi & c\phi s\theta c\psi + s\phi s\psi \\ c\theta s\phi & s\theta s\phi s\psi + c\psi c\phi & c\phi s\theta s\psi - c\psi s\phi \\ -s\theta & s\psi c\theta & c\phi c\theta \end{bmatrix} \quad (1)$$

where $c(*) = \cos(*)$ and $s(*) = \sin(*)$, for $* \in \phi, \theta, \psi$.

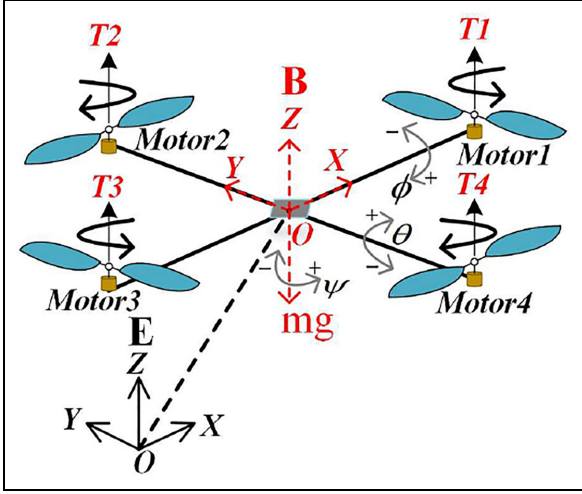


Figure 1. The schematic of the quadrotor.

The $\omega = [p, q, r]^T$ represents the angular velocity of the body. The relationship between the derivative of ζ and the angular velocity ω of the body is as follow:

$$\begin{aligned} \omega &= M_\zeta \dot{\zeta} \\ M_\zeta &= \begin{bmatrix} 1 & 0 & -\sin \theta \\ 0 & \cos \phi & \cos \theta \sin \phi \\ 0 & -\sin \phi & \cos \theta \cos \phi \end{bmatrix} \end{aligned} \quad (2)$$

The quadrotor flies in a steady environment, so the attitude changes approximately around zero. It means that $\theta \approx 0$, $\phi \approx 0$. M_ζ can become unit matrix so that we can conclude $\omega = \dot{\zeta}$.

According to Newton-Euler equation, the position and attitude dynamics equations are expressed as follows:

$$m\ddot{\xi} = C_B^E T_b - mge_z - k_p \dot{\xi} + d_p \quad (3)$$

$$J_b \dot{\omega} = -(\dot{\zeta} \times J_b \cdot \dot{\zeta}) + \tau_q - k_a \dot{\zeta} + d_a \quad (4)$$

where m presents the mass of the drone. g indicates the acceleration of gravity. $T_b = [0, 0, U_1]^T$. U_1 is the thrust input. $e_z = [0, 0, 1]^T$. $d_p = [d_x, d_y, d_z]^T$ and $d_a = [d_\phi, d_\theta, d_\psi]^T$ denote the external disturbances. $k_p = \text{diag}[k_1, k_2, k_3]$ and $k_a = \text{diag}[k_4, k_5, k_6]$ are the resistance coefficient matrix. $J_b = \text{diag}[J_{xx}, J_{yy}, J_{zz}]$ is the inertia matrix. $\tau_q = [U_2, U_3, U_4]^T$ represents torque input. The thrust input U_1 and torque input τ_q can be written as:

$$\begin{bmatrix} U_1 \\ U_2 \\ U_3 \\ U_4 \end{bmatrix} = \begin{bmatrix} b(\Omega_1^2 + \Omega_2^2 + \Omega_3^2 + \Omega_4^2) \\ lb(\Omega_2^2 - \Omega_4^2) \\ lb(\Omega_3^2 - \Omega_1^2) \\ \nu(\Omega_2^2 + \Omega_4^2 - \Omega_3^2 - \Omega_1^2) \end{bmatrix} \quad (5)$$

where l is the length of the quadrotor arm. $\Omega_i (i = 1, \dots, 4)$ denotes speed of each rotor. ν is a

positive drag constant. b is a positive coefficient. Therefore, the quadrotor dynamics equation can be described as:

$$\begin{cases} \ddot{x} = \frac{U_1}{m} (\sin \phi \sin \psi + \sin \theta \cos \phi \cos \psi) - k_1 \dot{x} + d_x \\ \ddot{y} = \frac{U_1}{m} (-\cos \psi \sin \phi + \cos \phi \sin \theta \sin \psi) - k_2 \dot{y} + d_y \\ \ddot{z} = \frac{U_1}{m} \cos \phi \cos \theta - g - k_3 \dot{z} + d_z \\ \ddot{\phi} = \frac{1}{J_{xx}} (\dot{\theta} \dot{\psi} (J_{yy} - J_{zz}) + U_2 - k_4 \dot{\phi}) + d_\phi \\ \ddot{\theta} = \frac{1}{J_{yy}} (\dot{\phi} \dot{\psi} (J_{zz} - J_{xx}) + U_3 - k_5 \dot{\theta}) + d_\theta \\ \ddot{\psi} = \frac{1}{J_{zz}} (\dot{\theta} \dot{\phi} (J_{xx} - J_{yy}) + U_4 - k_6 \dot{\psi}) + d_\psi \end{cases} \quad (6)$$

This paper aims to enable the quadrotor track the desired position $[x_d, y_d, z_d]^T$ and attitude $[\phi_d, \theta_d, \psi_d]^T$. In (6), the coupling of quadrotor is reflected in the coupling of position and attitude, and the coupling between attitudes. Due to under-actuation, we cannot use four inputs to track six degree-of-freedom. Therefore, the tracking of each channel in position is achieved separately by setting the virtual control law in position subsystem. The coupling between attitude and position is solved by designing virtual control laws of position, that is, the attitude information is included in virtual control laws of position. Further, the two desired attitude signals to the attitude subsystem are solved by virtual control of position subsystem. Attitude coupling is a known part of the controller if the model is accurate. Moreover, the unknown attitude coupling of the inner-loop can be overcome by the robustness of the controller. Meanwhile, the quadrotor becomes a double closed-loop system with an attitude inner-loop and a position outer-loop. We can analyze the stability of each degree of freedom of the inner and outer loops directly and ensure the stability of the inner and outer loops respectively, that is, the whole double closed-loop system is stable. The quadrotor can achieve the desired trajectory tracking. The virtual inputs $[U_x, U_y, U_z]^T$ for the position subsystem are defined as follows:

$$\begin{cases} U_x = (\sin \phi \sin \psi + \sin \theta \cos \phi \cos \psi) \frac{U_1}{m} \\ U_y = (-\cos \psi \sin \phi + \cos \phi \sin \theta \sin \psi) \frac{U_1}{m} \\ U_z = (\cos \phi \cos \theta) \frac{U_1}{m} - g \end{cases} \quad (7)$$

Then, the desired attitude angle (ϕ_d, θ_d) and U_1 are solved from the position loop as follows:

$$\begin{aligned} \phi_d &= \arctan \left(-\frac{\cos \psi_d U_y - \sin \psi_d U_x}{U_z + g} \cos \theta_d \right) \\ \theta_d &= \arctan \left(\frac{\cos \psi_d U_x + \sin \psi_d U_y}{U_z + g} \right) \\ U_1 &= m \sqrt{(U_z + g)^2 + U_x^2 + U_y^2} \end{aligned} \quad (8)$$

where $\psi_d \in (-\pi, \pi)$ is assigned by the users.

Remark 1. In (8), the results of desired ϕ_d, θ_d , thrust U_1 are solved by designed U_x, U_y, U_z . U_1 is the throttle provided by four motors, so $U_1 \geq 0$. The maximum of U_1 is determined by the motor quality, and the range of U_1 can be obtained by user instructions. Mathematically speaking, when $U_z = -g$, ϕ_d, θ_d will be singular. But $U_z = -g$ does not actually occur in normal flight, so (8) is reasonable. To ensure a safe and stable flight process, users generally ensure that attitude variation is minimal, that is, small angle condition and $\cos \phi \cos \theta > 0$, $U_z \geq -g$ in (7). So $U_1 = 0$ only when $U_z = -g$ (quadrotor is only subject to gravity and air resistance in sky). This represents the users suddenly shut power down or other accidents happen (shot down) in flight. This means that $U_z = -g$ does not occur in normal flight conditions because it is unreasonable for users to provide a trajectory equaling to the free-fall motion, thus (8) is reasonable. All controllers satisfying the stability analysis can track the desired trajectory and $U_z \neq -g$, as long as the desired trajectory is not free-fall motion.

Remark 2. To prevent singularities of (8) in calculation, we can also make $|U_z| < g$ by anti-saturation in the subsequent design process, and allocate U_x and U_y reasonably to ensure that U_1 does not exceed the maximum lift. Just make sure that the lift range includes gravity, and the maximum lift is greater than gravity to ensure that the quadrotor can ascend as well as descend. Adjusting the controller parameters will affect the controller dynamic performance and tracking effect, but does not change the reasonableness of (8). When the controller is valid and the controller parameters meet the tuning rules, then the desired attitude change is largely influenced by the desired position change given by the user and attitude make small changes in stable situation.

The position and attitude subsystems of the quadrotor are second-order nonlinear systems, which we describe in particular by the following set of equations:

$$\begin{aligned}\dot{h}_n &= h_{n+1} \quad (n = 1, 3, 5, 7, 9, 11) \\ h_{n+1} &= f(h) + p(h)U + \Delta g(h) + d_v \quad (v = x, y, z, \phi, \theta, \psi)\end{aligned}\quad (9)$$

where $p(h), f(h)$ are known bounded nonlinear functions. U denotes the control inputs of second-order nonlinear systems. d_v denotes external disturbances which is bound by a constant. $\Delta g(h)$ denotes unmodeled dynamics determined by the system states. Thus, the total uncertainty $d_v + \Delta g(h)$ has a clear physical meaning and is bounded. The upper bound information of $\Delta g(h)$ is related to position, velocity and acceleration for quadrotor. Acceleration signal is difficult to measure in practice so that upper bound information related to acceleration can still be expressed as a constant and upper bounds for

unmodeled dynamics can be provided from position and velocity measurements. So both the uncertainty and its upper bound can be simply constructed as the form with the system state attached. This approach can effectively deal with nonparametric uncertainty and time-varying parameters. The $\Delta g(h)$ can be constructed and satisfies: $\Delta g(h) = \Delta p_0 + \Delta p_1 h_n + \Delta p_2 h_{n+1} \leq |\Delta p_0| + |\Delta p_1||h_n| + |\Delta p_2||h_{n+1}|$ where $\Delta p_0, \Delta p_1, \Delta p_2$ are additive physical parameter uncertainties and Δp_0 independent of system states. It is obvious that the upper bounds of $\Delta p_0, \Delta p_1, \Delta p_2$ are unknown and existing. The upper bound of total uncertainty can be assumed as $L_{v0} + L_{v1}|v| + L_{v2}|\dot{v}|$, where L_{v0}, L_{v1}, L_{v2} are unknown and existing positive constant.^{31,32} This assumption exists and specifies the practical implications of the upper bound on uncertainty and is well suited for adaptive controller design. We do not need to know their details and just estimate them adaptively, then we can get:

$$|\Delta g(h) + d| \leq L_{v0} + L_{v1}|v| + L_{v2}|\dot{v}| \quad (v = x, y, z, \phi, \theta, \psi) \quad (10)$$

Remark 3. According to the dynamics of rigid-body robots, (10) is reasonable and used by many researchers.^{15,33} This assumption is a general assumption describing an unknown upper bound on the dynamics of a rigid-body robot. The plausibility of the practical meaning in (10) is as follows³⁴: The first term L_{v0} presents unknown time-varying disturbances such as wind, resonance, and rotor turbulence. The second term $L_{v1}|v|$ presents unknown forces due to mechanical stiffness and unknown friction. The third term $L_{v2}|\dot{v}|$ presents unknown torque due to Coriolis forces and unmodeled gyroscopic moment of four rotors.

Equation (9) can be obtained as follows:

$$\left\{ \begin{array}{l} \dot{h}_1 = h_2 \\ h_2 = (\sin h_7 \sin h_{11} + \cos h_7 \sin h_9 \cos h_{11}) \frac{U_1}{m} \\ \quad - k_1 h_2 + d_x = U_x - k_1 h_2 + d_x \\ \dot{h}_3 = h_4 \\ h_4 = (-\sin h_7 \cos h_{11} + \cos h_7 \sin h_9 \sin h_{11}) \frac{U_1}{m} \\ \quad - k_2 h_4 + d_y = U_y - k_2 h_4 + d_y \\ \dot{h}_5 = h_6 \\ h_6 = (\cos h_7 \cos h_9) \frac{U_1}{m} - k_3 h_6 - g + d_z \\ \quad = U_z - k_3 h_6 + d_z \\ \dot{h}_7 = h_8 \\ h_8 = q_1 h_{10} h_{12} + w_1 U_2 - k_4 w_1 h_8 + d_\phi \\ \dot{h}_9 = h_{10} \\ h_{10} = q_2 h_8 h_{12} + w_2 U_3 - k_5 w_2 h_{10} + d_\theta \\ \dot{h}_{11} = h_{12} \\ h_{12} = q_3 h_8 h_{10} + w_3 U_4 - k_6 w_3 h_{12} + d_\psi \end{array} \right. \quad (11)$$

the coefficients are taken as:
 $q_1 = \frac{J_{yy}-J_{zz}}{J_{xx}}, q_2 = \frac{J_{zz}-J_{xx}}{J_{yy}}, q_3 = \frac{J_{xx}-J_{yy}}{J_{zz}}, w_1 = \frac{1}{J_{xx}}, w_2 = \frac{1}{J_{yy}}, w_3 = \frac{1}{J_{zz}}$

Further, the control inputs provided by the actuator is bounded, and ideal inputs with high gain are not realistic. For this reason, we constrain the control inputs and ensure that the system is stable. At this time, U_i is the bounded actual control input, which can be written as:

$$U_i = \text{sats}(U_i^*)(i = x, y, z, 2, 3, 4) \quad (12)$$

where the $\text{sats}(U_i^*)$ is defined as:

$$\text{sats}(U_i^*) = \begin{cases} U_{imax}, & U_i^* > U_{imax} \\ U_i^*, & |U_i^*| \leq U_{imax} \\ -U_{imax}, & U_i^* < -U_{imax} \end{cases} \quad (13)$$

where $U_{imax} > 0$, U_i^* is the unconstrained ideal control input, then we get:

$$U_i = \text{sats}(U_i^*) = U_i^* + \delta_v \quad (14)$$

To solve the actuator saturation,³⁵ we proposed an anti-saturation auxiliary compensator as follows:

$$\dot{\hat{\delta}}_v = \begin{cases} -\bar{c}_v \hat{\delta}_v + p(h)\sigma_v - \frac{|p(h)\sigma_v \delta_v| + \frac{1}{2}\delta_v^2}{|\delta_v|^2} \hat{\delta}_v \\ + \delta_v, \text{ for } |\hat{\delta}_v| \geq \hat{\delta}_{vr} \text{ or } \delta_v \neq 0 \\ 0, \text{ for } |\hat{\delta}_v| < \hat{\delta}_{vr} \text{ and } \delta_v = 0 \end{cases} \quad (15)$$

where δ_v ($v = x, y, z, \phi, \theta, \psi$) denotes saturation errors between actual input U_i and ideal input U_i^* . $\hat{\delta}_v$ is the state of the auxiliary system which compensates the saturation errors. $p(h)$ are known bounded nonlinear functions. σ_v presents the sliding mode surface. \bar{c}_v is a design parameter, and $\hat{\delta}_{vr}$ is a small positive constant.

In order to guarantee $\hat{\delta}_v \rightarrow 0$ as $t \rightarrow 0$, it is necessary for $\bar{c}_v > 0$ to meet Hurwitz requirement. This compensator is dynamically adjusted according to δ_v and combined with the controller to solve the input saturation. By choosing a suitable \bar{c}_v and using Lyapunov direct method, the compensator state $\hat{\delta}_v$ can converge to 0 stably and the boundedness of $\hat{\delta}_v$ in ideal input U_i^* can be ensured. Then the ideal U_i^* is bounded based on Lyapunov direct method means that δ_v is bounded.

The $e = [e_1, e_2, \dots, e_{12}]^T \in \mathbf{R}^{12}$ defines the errors of trajectory tracking respecting to position and attitude, which is as follows:

$$\begin{bmatrix} e_1 \\ e_2 \\ e_3 \\ e_4 \\ e_5 \\ e_6 \end{bmatrix} = \begin{bmatrix} h_1 - x_d \\ h_2 - \dot{x}_d \\ h_3 - y_d \\ h_4 - \dot{y}_d \\ h_5 - z_d \\ h_6 - \dot{z}_d \end{bmatrix}, \begin{bmatrix} e_7 \\ e_8 \\ e_9 \\ e_{10} \\ e_{11} \\ e_{12} \end{bmatrix} = \begin{bmatrix} h_7 - \phi_d \\ h_8 - \dot{\phi}_d \\ h_9 - \theta_d \\ h_{10} - \dot{\theta}_d \\ h_{11} - \psi_d \\ h_{12} - \dot{\psi}_d \end{bmatrix} \quad (16)$$

Controller design

This section gives the design process of the NDOB-AFNTSM controller. The proposed method enables quadrotor to accomplish stable, fast, and accurate trajectory tracking under complex external disturbances, actuator saturation and unmodeled dynamics. Figure 2 shows the NDOB-AFNTSM scheme in this paper. The control structure is divided into the inner-loop attitude subsystem and the outer-loop position subsystem. The outer-loop combines the NDOB and the new reaching law (NRL). The adaptive method estimates the unknown upper bound respecting to the NDOB errors online in the outer-loop. In the inner-loop, the unknown upper bounds of the external disturbances are estimated by adaptive laws. The anti-saturation auxiliary compensator is to compensate for unknown saturation errors for solving the problem of actuator saturation. Tracking error converges in finite time based on fast non-singular sliding surfaces. The proposed method improves the control accuracy and robustness while suppressing chattering adequately. The specific design procedure is described in the following subsections.

Design of the position controller

This part is to design the virtual inputs (U_x, U_y, U_z) of the position subsystem. Based on equation (9), the second-order position subsystem is given as follows:

$$\begin{aligned} \dot{h}_n &= h_{n+1} & (n = 1, 3, 5) \\ \dot{h}_{n+1} &= f(h) + p(h)U + d_v & (v = x, y, z) \end{aligned} \quad (17)$$

The nonlinear disturbance observer is as follows³⁶:

$$\begin{cases} \dot{\varrho} = -\epsilon\varrho - \epsilon[\epsilon h_{n+1} + f(h) + p(h)U] \\ \dot{\hat{d}}_v = \varrho + \epsilon h_{n+1} \end{cases} \quad (18)$$

where \hat{d}_v is the estimation of d_v . ϱ denotes the state vector of the NDOB, and ϵ is the positive observer bandwidth. U presents the control inputs of second-order position subsystem.

The error of estimated d_v and its derivative are defined as:

$$\begin{cases} \tilde{d}_v = d_v - \hat{d}_v \\ \dot{\tilde{d}}_v = \dot{d}_v - \dot{\hat{d}}_v \end{cases} \quad (19)$$

The derivative of \hat{d}_v is follow:

$$\begin{aligned} \dot{\hat{d}}_v &= \dot{\varrho} + \epsilon \dot{h}_{n+1} \\ &= -\epsilon\varrho - \epsilon[\epsilon h_{n+1} + f(h) + p(h)U] \\ &\quad + \epsilon[f(h) + p(h)U + d_v] \\ &= -\epsilon(\varrho + \epsilon h_{n+1}) + \epsilon d_v \\ &= -\epsilon(\hat{d}_v - d_v) \\ &= \epsilon \tilde{d}_v \end{aligned} \quad (20)$$

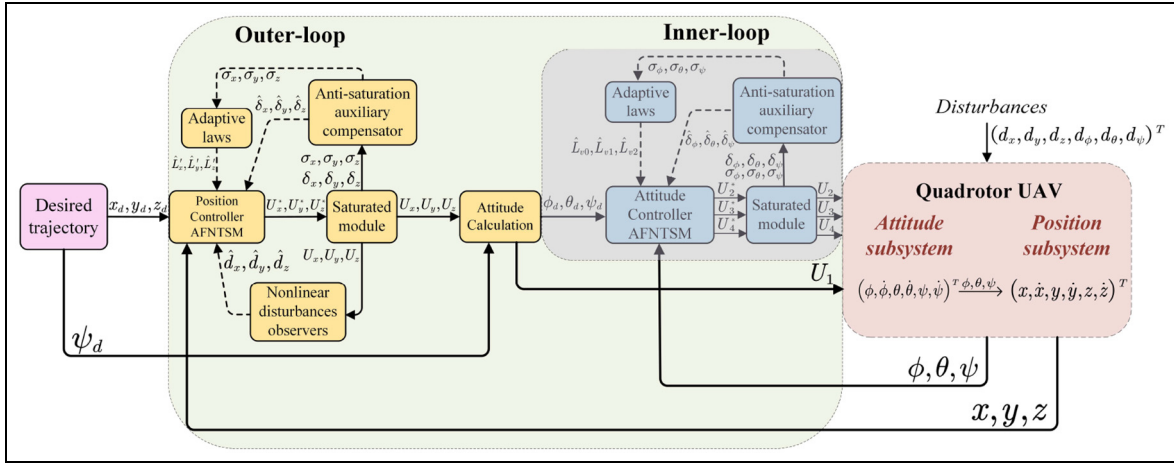


Figure 2. Control system block diagram.

Define a Lyapunov function as follows:

$$V_d = \frac{1}{2} \tilde{d}_v^2 \quad (21)$$

The derivative of V_d is:

$$\dot{V}_d = \tilde{d}_v \dot{\tilde{d}}_v = \tilde{d}_v (\dot{d}_v - \dot{\tilde{d}}_v) = \tilde{d}_v (\dot{d}_v - \epsilon \tilde{d}_v) = -\epsilon \tilde{d}_v^2 + \dot{d}_v \tilde{d}_v \quad (22)$$

According to the basic inequality:

$$\dot{d}_v \tilde{d}_v \leq \frac{1}{2} \dot{d}_v^2 + \frac{1}{2} \tilde{d}_v^2 \quad (23)$$

For equation (22), we have:

$$\begin{aligned} \dot{V}_d &\leq -\epsilon \tilde{d}_v^2 + \frac{1}{2} (\tilde{d}_v^2 + \dot{d}_v^2) = -(\epsilon - \frac{1}{2}) \tilde{d}_v^2 + \frac{1}{2} \dot{d}_v^2 \\ &= -(2\epsilon - 1) V_d + \frac{1}{2} \dot{d}_v^2 \end{aligned} \quad (24)$$

In general, we do not have information about disturbances and their derivatives. But real-world signals are always bounded signals with finite energy, it means that a signal with a specific physical meaning cannot diverge in reality, which is an objective reality. Further, external disturbances to the quadrotor are generally smooth and continuous low to medium frequency signals such as wind, resonance, and rotor turbulence. We can consider that the variation of the disturbances is small relative to the observer dynamics. Based on the above motivations, we can give the following assumption.

Assumption 3.³⁷ $d_v (v = x, y, z)$ is the bounded disturbances, and its derivative satisfies:

$$|\dot{d}_v| \leq \epsilon_d. \quad (25)$$

where ϵ_d is a small positive constant. This is a common assumption for designing nonlinear disturbances observer.

Lemma 1.³⁸ For a positive definite function V : $[0, +\infty) \in R$, The solution for $\dot{V} \leq -\alpha V + \eta$, $\forall t \geq t_0 \geq 0$ is:

$$V(t) \leq V(t_0) e^{-\alpha(t-t_0)} + \int_{t_0}^t e^{-\alpha(t-\tau)} \eta(\tau) d\tau \quad (26)$$

where $0 \leq \eta < +\infty$, $\alpha > 0$. The V is stable and ultimately bounded.

According to Lemma 1 and Assumption 3, the effect of the disturbance derivative in (24) is very small, and the relatively large bandwidth ϵ can be chosen to offset the effect of the disturbance derivative. V_d is stable and the observer error converges to a very small domain. This NDOB is effective for some fast-varying disturbances provided that the disturbance derivative is bounded.³⁷

The fast nonsingular terminal sliding surfaces for the position subsystem is as follows:

$$\begin{aligned} \sigma_x &= e_2 + \alpha_1 e_1 + \beta_1 |e_1|^{c_1} \text{sign}(e_1) \\ \sigma_y &= e_4 + \alpha_3 e_3 + \beta_3 |e_3|^{c_3} \text{sign}(e_3) \\ \sigma_z &= e_6 + \alpha_5 e_5 + \beta_5 |e_5|^{c_5} \text{sign}(e_5) \end{aligned} \quad (27)$$

where $1 < c_i < 2$, $\alpha_i, \beta_i > 0$ ($i = 1, 3, 5$) are positive numbers.

Substituting equations (7), (11), and (14) into equation (27), the derivatives of the sliding surfaces can be expressed as:

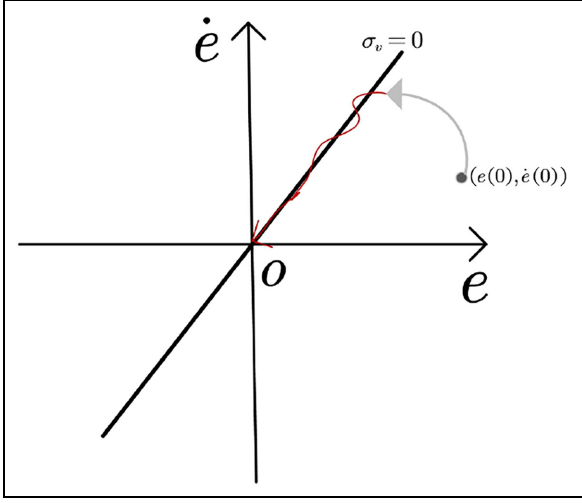


Figure 3. Sliding-mode principle.

$$\begin{aligned}\dot{\sigma}_x &= U_x^* + \delta_x - k_1 h_2 + d_x - \ddot{x}_d + \alpha_1 e_2 + \beta_1 c_1 |e_1|^{c_1-1} e_2 \\ \dot{\sigma}_y &= U_y^* + \delta_y - k_2 h_4 + d_y - \ddot{y}_d + \alpha_3 e_4 + \beta_3 c_3 |e_3|^{c_3-1} e_4 \\ \dot{\sigma}_z &= U_z^* + \delta_z - k_3 h_6 + d_z - \ddot{z}_d + \alpha_5 e_6 + \beta_5 c_5 |e_5|^{c_5-1} e_6\end{aligned}\quad (28)$$

The control law is composed of switching control U_{swv}^* and equivalent control U_{eqv}^* , with the following expression:

$$U_v^* = U_{swv}^* + U_{eqv}^* \quad (v = x, y, z) \quad (29)$$

Let $\dot{\sigma}_v = 0$ ($v = x, y, z$), we can conclude the U_{eqv}^* as:

$$\begin{aligned}U_{eqx}^* &= k_1 h_2 - \hat{d}_x + \ddot{x}_d - \alpha_1 e_2 - \beta_1 c_1 |e_1|^{c_1-1} e_2 - \hat{\delta}_x \\ U_{eqy}^* &= k_2 h_4 - \hat{d}_y + \ddot{y}_d - \alpha_3 e_4 - \beta_3 c_3 |e_3|^{c_3-1} e_4 - \hat{\delta}_y \\ U_{eqz}^* &= k_3 h_6 - \hat{d}_z + \ddot{z}_d - \alpha_5 e_6 - \beta_5 c_5 |e_5|^{c_5-1} e_6 - \hat{\delta}_z\end{aligned}\quad (30)$$

where $\hat{\delta}_x, \hat{\delta}_y, \hat{\delta}_z$ are the compensated saturation errors.

The sliding mode motion is divided into two phases: reaching motion and sliding motion. Figure 3 shows the sliding-mode principle in phase diagram. The first phase is the reaching process: $\sigma_v \rightarrow 0$. The dynamic quality of this phase plays a crucial role because the system state can be forced to 0 on the sliding mode surface only by ensuring that the reaching motion is effective. Choosing a suitable reaching law can improve the dynamic quality of the system and ensure a fast response when the system state is far away from the sliding surface. The common reaching laws are isokinetic law, exponential law, and power law.³⁹ These methods are difficult to combine both anti-chattering and rapidity. For example, the exponential law is not suitable for solving the situation where the initial errors is small, which can cause

unnecessary chattering. To solve above problem, we propose an improved new reaching law based on the work by Napole et al.⁴⁰ NRL retaining the advantages of the double power reaching law, we replace the constant part of exponent with a logarithmic function related to the state of the system and enhance anti-chattering capability. Furthermore, NRL can maintain a speed as small as possible when the system state is very close to the surface. NRL is given by:

$$\dot{\sigma}_v = -[\lambda_1(b_v^{|\sigma_v|} - 1) + \lambda_2 |\sigma_v|^{\ln(1+|\sigma_v|)} + (L'_v + \eta)] \text{sign}(\sigma_v) \quad (v = x, y, z) \quad (31)$$

where $b_v > 1$, $\lambda_i > 0$ ($i = 1, 2$), $\eta > 0$, $L'_v \geq \tilde{d}_v$, L'_v is the upper bound of NDOB error that is an unknown positive constant.

For the reaching law in (31), we give the following analysis: Firstly, (31) can ensure $\sigma_v \dot{\sigma}_v < 0$. If the system state is far away from the sliding mode surface, that is, $|\sigma_v| > \exp(1) - 1$, then $\ln(1 + |\sigma_v|) > 1$, the rapidity of the system state is mainly determined by the variable index term and the variable power term, which can ensure a larger speed. Besides, if $|\sigma_v|$ decreases, then $b^{|\sigma_v|} - 1$ and $|\sigma_v|^{\ln(1+|\sigma_v|)}$ quickly converge to small constants. This means that chattering reduces in reaching phase. If system state is extremely close to the sliding mode surface, that is, $|\sigma_v| < \exp(1) - 1$, then $\ln(1 + |\sigma_v|) < 1$, the convergence speed is determined by constant term $L'_v + \eta$, and $L'_v + \eta$ should be as small as possible, which ensures that state reaches sliding mode surface in finite time. Thus, NRL is faster than common reaching laws in the whole process from the initial state to the sliding-mode surface. Then the switching control laws in position system can be provided as:

$$U_{swv}^* = -[\lambda_{1v}(b_v^{|\sigma_v|} - 1) + \lambda_{2v} |\sigma_v|^{\ln(1+|\sigma_v|)} + (\hat{L}'_v + \eta_v)] \text{sign}(\sigma_v) \quad (32)$$

where $b_v, \lambda_{1v}, \lambda_{2v}$ and η_v ($v = x, y, z$) are positive parameters, $\hat{L}'_x, \hat{L}'_y, \hat{L}'_z$ are the estimated upper bound of the NDOB errors. The adaptive laws for position subsystem is as follows:

$$\dot{\hat{L}}'_v = \mu_v |\sigma_v| \quad (33)$$

where $\mu_v > 0$ ($v = x, y, z$).

Remark 4.³³ Due to sensor noise, system inertia, etc., σ_v ($v = x, y, z$) moves around zero. This causes the \hat{L}'_v to become larger all the time. To prevent the controllers from divergence problem, we use the dead zone method to give corrections to the adaptive laws:

$$\dot{\hat{L}}'_v = \begin{cases} \mu_v |\sigma_v|, & \text{for } |\sigma_v| \geq \varepsilon \\ 0, & \text{for } |\sigma_v| < \varepsilon \end{cases} \quad (34)$$

The \hat{L}'_v will not grow under $|\sigma_v| < \varepsilon$ ($\varepsilon > 0$, ε is a small threshold designed as 0.1 in our case). it is clear that \hat{L}'_v keep present value when σ_v in this small threshold.

The virtual inputs U_x^* , U_y^* , and U_z^* can be presented as:

$$\left\{ \begin{array}{l} U_x^* = k_1 h_2 - \hat{d}_x + \ddot{x}_d - \alpha_1 e_2 - \beta_1 c_1 |e_1|^{c_1-1} e_2 \\ \quad - \hat{\delta}_x - [\lambda_{1x}(b_x^{|\sigma_x|} - 1) + \lambda_{2x} |\sigma_x|^{\ln(1+|\sigma_x|)} \\ \quad + (\hat{L}'_x + \eta_x)] \text{sign}(\sigma_x) \\ U_y^* = k_2 h_4 - \hat{d}_y + \ddot{y}_d - \alpha_3 e_4 - \beta_3 c_3 |e_3|^{c_3-1} e_4 \\ \quad - \hat{\delta}_y - [\lambda_{1y}(b_y^{|\sigma_y|} - 1) + \lambda_{2y} |\sigma_y|^{\ln(1+|\sigma_y|)} \\ \quad + (\hat{L}'_y + \eta_y)] \text{sign}(\sigma_y) \\ U_z^* = k_3 h_6 - \hat{d}_z + \ddot{z}_d - \alpha_5 e_6 - \beta_5 c_5 |e_5|^{c_5-1} e_6 \\ \quad - \hat{\delta}_z - [\lambda_{1z}(b_z^{|\sigma_z|} - 1) + \lambda_{2z} |\sigma_z|^{\ln(1+|\sigma_z|)} \\ \quad + (\hat{L}'_z + \eta_z)] \text{sign}(\sigma_z) \end{array} \right. \quad (35)$$

Lemma 2.³³ Consider a system that satisfies the following first-order nonlinear inequality:

$$\dot{V}(h) + \varsigma V^\gamma(h) \leq 0 \quad (36)$$

where $0 < \gamma < 1$, $\varsigma > 0$, $V(h)$ denotes a positive Lyapunov function, $h \in R$ represents the state of system. System converges in the finite time. The convergence time from $V(h(0))$ to zero can be calculated as:

$$t_a \leq \frac{V^{1-\gamma}(h(0))}{\varsigma(1-\gamma)} \quad (37)$$

Theorem 1. Considering the x -subsystem (6) with the surface (27) and the anti-saturation auxiliary compensator (15). The controllers and the adaptive laws are designed as (35) and (33)–(34). The system is uniformly bounded stable and σ_x converges asymptotically to 0, then the following statements hold:

- i) The error e_1 converges to zero in a finite time;
- ii) All signals of the x -subsystem (6) are bounded.

Proof. Define a Lyapunov function as follows:

$$V_x = \frac{1}{2} \sigma_x^2 + \frac{1}{2} \hat{\delta}_x^2 + \frac{1}{2\mu_x} \tilde{L}_x^2 \quad (38)$$

where $\tilde{L}'_x = \hat{L}'_x - L'_x$, $\mu_x > 0$.

The derivative of V_x is:

$$\dot{V}_x = \sigma_x \dot{\sigma}_x + \hat{\delta}_x \dot{\hat{\delta}}_x + \frac{1}{\mu_x} \tilde{L}_x \dot{\tilde{L}}_x \quad (39)$$

Substituting the equation (15) into equation (39), we can obtain:

$$\begin{aligned} \dot{V}_x &= \sigma_x (\tilde{d}_x - \hat{\delta}_x + \delta_x - [\lambda_{1x}(b_x^{|\sigma_x|} - 1) \\ &\quad + \lambda_{2x} |\sigma_x|^{\ln(1+|\sigma_x|)} + (\hat{L}'_x + \eta_x)] \text{sign}(\sigma_x)) \\ &\quad + \hat{\delta}_x (-\bar{c}_x \hat{\delta}_x + \sigma_x - \frac{|\sigma_x \delta_x| + \frac{1}{2} \delta_x^2}{|\hat{\delta}_x|^2} \hat{\delta}_x + \delta_x) \\ &\quad + \frac{1}{\mu_x} (\hat{L}'_x - L'_x) \dot{\hat{L}}_x \end{aligned} \quad (40)$$

$$\begin{aligned} &= \sigma_x \tilde{d}_x - (\lambda_{1x}(b_x^{|\sigma_x|} - 1) + \lambda_{2x} |\sigma_x|^{\ln(1+|\sigma_x|)} \\ &\quad + (\hat{L}'_x + \eta_x)) |\sigma_x| + \sigma_x \delta_x - \bar{c}_x \hat{\delta}_x^2 + \hat{\delta}_x \delta_x \\ &\quad - |\sigma_x \delta_x| - \frac{1}{2} \delta_x^2 + \frac{1}{\mu_x} (\hat{L}'_x - L'_x) \dot{\hat{L}}_x \end{aligned} \quad (41)$$

Substituting the equation (33) into equation (41), then we get:

$$\begin{aligned} \dot{V}_x &= \sigma_x \tilde{d}_x - (\lambda_{1x}(b_x^{|\sigma_x|} - 1) + \lambda_{2x} |\sigma_x|^{\ln(1+|\sigma_x|)} \\ &\quad + (\hat{L}'_x + \eta_x)) |\sigma_x| + \sigma_x \delta_x - \bar{c}_x \hat{\delta}_x^2 + \hat{\delta}_x \delta_x \\ &\quad - |\sigma_x \delta_x| - \frac{1}{2} \delta_x^2 \\ &\leq |\sigma_x| (|\tilde{d}_x| - (\lambda_{1x}(b_x^{|\sigma_x|} - 1) + \lambda_{2x} |\sigma_x|^{\ln(1+|\sigma_x|)} \\ &\quad + (\hat{L}'_x + \eta_x))) - \bar{c}_x \hat{\delta}_x^2 - \frac{1}{2} \delta_x^2 + \hat{\delta}_x \delta_x \end{aligned} \quad (42)$$

According to the basic inequality:

$$\hat{\delta}_x \delta_x \leq \frac{1}{2} \hat{\delta}_x^2 + \frac{1}{2} \delta_x^2 \quad (43)$$

$$\begin{aligned} \dot{V}_x &\leq |\sigma_x| (|\tilde{d}_x| - (\lambda_{1x}(b_x^{|\sigma_x|} - 1) + \lambda_{2x} |\sigma_x|^{\ln(1+|\sigma_x|)} \\ &\quad + (\hat{L}'_x + \eta_x))) - \left(\bar{c}_x - \frac{1}{2} \right) \hat{\delta}_x^2 \end{aligned} \quad (44)$$

Noting that in equation (44), because of (31), the $b_x > 1$, $\lambda_{ix} > 0$ ($i = 1, 2$), $\eta_x > 0$, $L'_x \geq |\tilde{d}_x|$, then we can get:

$$\begin{aligned} &\lambda_{1x}(b_x^{|\sigma_x|} - 1) + \lambda_{2x} |\sigma_x|^{\ln(1+|\sigma_x|)} + (\hat{L}'_x + \eta_x) \\ &> L'_x + \eta_x > |\tilde{d}_x| > 0 \end{aligned} \quad (45)$$

Besides, \bar{c}_x is a design parameter, it can be chosen to satisfy the condition $\bar{c}_x > \frac{1}{2}$ ensures that $-(\bar{c}_x - \frac{1}{2}) \hat{\delta}_x^2 \leq 0$.

To sum up, we get:

$$\dot{V}_x \leq |\sigma_x| (|\tilde{d}_x| - (L'_x + \eta_x)) \leq 0 \quad (46)$$

Obviously, V_x is positive definite and lower bounded, \dot{V}_x is negative semi-definite. In the initial condition $V_x(t) \leq V_x(0)$, V_x is bounded, so e_1 , \tilde{L}_x , σ_x and $\hat{\delta}_x$ are proved to be bounded when $t \rightarrow \infty$, then we can

conclude U_x^* and δ_x are bounded. $\sigma_x \neq 0$, $\dot{V}_x < 0$. So $t \rightarrow \infty$, $\sigma_x \rightarrow 0$, $\dot{V}_x \rightarrow 0$. When $\sigma_x = 0$, $\dot{V}_x = 0$, \tilde{L}'_x and $\hat{\delta}_x$ keep static. In summary, we obtain that σ_x converges asymptotically to 0, the x -system is uniformly bounded stable and all signals are eventually bounded. Further, when the system is on $\sigma_x = 0$, for the system $\dot{e}_1 = -\alpha_1 e_1 - \beta_1 |e_1|^{c_1} \text{sign}(e_1)$, define the Lyapunov function $V'_x = \frac{1}{2} e_1^2$, we have:

$$\begin{aligned}\dot{V}'_x &= e_1 \dot{e}_1 \\ &= -\alpha_1 e_1^2 - \beta_1 |e_1|^{c_1+1} \\ &\leq -(\alpha_1 |e_1| + \beta_1 |e_1|^{c_1}) \sqrt{2} \frac{|e_1|}{\sqrt{2}} \\ &= -\sqrt{2} \zeta V'_x(t)\end{aligned}\quad (47)$$

where $\zeta = \alpha_1 |e_1| + \beta_1 |e_1|^{c_1}$. According to the Lemma 2, e_1 converges to zero in the finite time and:

$$t_p \leq \frac{\sqrt{2} V'_x(0)}{\zeta} \quad (48)$$

Finally, the x -system uniformly bounded stability is ensured and all signals of x -system are bounded. The y -system, z -system are uniformly bounded stable by using similar proof methods and the process is omitted here. This completes the proof.

Theorem 2. The position subsystem is uniformly bounded stable under the controllers U_x^* , U_y^* , and U_z^* .

Proof. A Lyapunov function is defined as follows:

$$\begin{aligned}V_p &= V_x + V_y + V_z \\ &= \frac{1}{2} \sigma_x^2 + \frac{1}{2} \hat{\delta}_x^2 + \frac{1}{2\mu_x} \tilde{L}'_x^2 + \frac{1}{2} \sigma_y^2 + \frac{1}{2} \hat{\delta}_y^2 + \frac{1}{2\mu_y} \tilde{L}'_y^2 \\ &\quad + \frac{1}{2} \sigma_z^2 + \frac{1}{2} \hat{\delta}_z^2 + \frac{1}{2\mu_z} \tilde{L}'_z^2\end{aligned}\quad (49)$$

The derivative of V_p is:

$$\begin{aligned}\dot{V}_p &= \sigma_x \dot{\sigma}_x + \hat{\delta}_x \dot{\hat{\delta}}_x + \frac{1}{\mu_x} \tilde{L}'_x \dot{\tilde{L}}'_x + \sigma_y \dot{\sigma}_y + \hat{\delta}_y \dot{\hat{\delta}}_y + \frac{1}{\mu_y} \tilde{L}'_y \dot{\tilde{L}}'_y \\ &\quad + \sigma_z \dot{\sigma}_z + \hat{\delta}_z \dot{\hat{\delta}}_z + \frac{1}{\mu_z} \tilde{L}'_z \dot{\tilde{L}}'_z\end{aligned}\quad (50)$$

Simplifying above equation and replacing the (15), (33) into equation (50), it yields:

$$\begin{aligned}\dot{V}_p &\leq |\sigma_x|(|\tilde{d}_x| - (\lambda_{1x}(b_x^{|\sigma_x|} - 1) \\ &\quad + \lambda_{2x}|\sigma_x|^{\ln(1+|\sigma_x|)} + (L'_x + \eta_x))) \\ &\quad + |\sigma_y|(|\tilde{d}_y| - (\lambda_{1y}(b_y^{|\sigma_y|} - 1) \\ &\quad + \lambda_{2y}|\sigma_y|^{\ln(1+|\sigma_y|)} + (L'_y + \eta_y))) \\ &\quad + |\sigma_z|(|\tilde{d}_z| - (\lambda_{1z}(b_z^{|\sigma_z|} - 1) \\ &\quad + \lambda_{2z}|\sigma_z|^{\ln(1+|\sigma_z|)} + (L'_z + \eta_z))) \\ &\leq |\sigma_x|(|\tilde{d}_x| - (L'_x + \eta_x)) + |\sigma_y|(|\tilde{d}_y| - (L'_y + \eta_y)) \\ &\quad + |\sigma_z|(|\tilde{d}_z| - (L'_z + \eta_z)) \leq 0\end{aligned}\quad (51)$$

From the previous analysis, it follows that the position subsystem is uniformly bounded stable.

Design of the attitude controller

This part will adopt the AFNTSM approach to control the inner-loop and force the system state (h_7, h_9, h_{11}) to converge to the desired value $(\phi_d, \theta_d, \psi_d)$ in a finite time. The sliding mode surfaces for attitude loop are as follows:

$$\begin{aligned}\sigma_\phi &= e_8 + \alpha_7 e_7 + \beta_7 |e_7|^{\frac{p_7}{q_7}} \text{sign}(e_7) \\ \sigma_\theta &= e_{10} + \alpha_9 e_9 + \beta_9 |e_9|^{\frac{p_9}{q_9}} \text{sign}(e_9) \\ \sigma_\psi &= e_{12} + \alpha_{11} e_{11} + \beta_{11} |e_{11}|^{\frac{p_{11}}{q_{11}}} \text{sign}(e_{11})\end{aligned}\quad (52)$$

where $\alpha_i, \beta_i > 0$ ($i = 7, 9, 11$), $p_i, q_i > 0$ ($1 < \frac{p_i}{q_i} < 2$) are positive odd parameters.

Substituting equations (11) and (14) into equation (52), the derivative of the sliding mode surfaces are offered as follows:

$$\begin{aligned}\dot{\sigma}_\phi &= q_1 h_{10} h_{12} + w_1 (U_2^* + \delta_\phi) - k_4 w_1 h_8 + d_\phi \\ &\quad - \dot{\phi}_d + \alpha_7 e_8 + \beta_7 \frac{p_7}{q_7} |e_7|^{\frac{p_7}{q_7}-1} e_8 \\ \dot{\sigma}_\theta &= q_2 h_8 h_{12} + w_2 (U_3^* + \delta_\theta) - k_5 w_2 h_{10} + d_\theta \\ &\quad - \ddot{\theta}_d + \alpha_9 e_{10} + \beta_9 \frac{p_9}{q_9} |e_9|^{\frac{p_9}{q_9}-1} e_{10} \\ \dot{\sigma}_\psi &= q_3 h_8 h_{10} + w_3 (U_4^* + \delta_\psi) - k_6 w_3 h_{12} + d_\psi \\ &\quad - \ddot{\psi}_d + \alpha_{11} e_{12} + \beta_{11} \frac{p_{11}}{q_{11}} |e_{11}|^{\frac{p_{11}}{q_{11}}-1} e_{12}\end{aligned}\quad (53)$$

By configuring $\dot{\sigma}_v = 0$ ($v = \phi, \theta, \psi$), we can get the equivalent control laws U_{eqv}^* ($v = 2, 3, 4$) as follows:

$$\begin{aligned}U_{eq2}^* &= \frac{1}{w_1} (k_4 w_1 h_8 + \ddot{\phi}_d - q_1 h_{10} h_{12} - \alpha_7 e_8 \\ &\quad - \beta_7 \frac{p_7}{q_7} |e_7|^{\frac{p_7}{q_7}-1} e_8) - \hat{\delta}_\phi \\ U_{eq3}^* &= \frac{1}{w_2} (k_5 w_2 h_{10} + \ddot{\theta}_d - q_2 h_8 h_{12} - \alpha_9 e_{10} \\ &\quad - \beta_9 \frac{p_9}{q_9} |e_9|^{\frac{p_9}{q_9}-1} e_{10}) - \hat{\delta}_\theta \\ U_{eq4}^* &= \frac{1}{w_3} (k_6 w_3 h_{12} + \ddot{\psi}_d - q_3 h_8 h_{10} - \alpha_{11} e_{12} \\ &\quad - \beta_{11} \frac{p_{11}}{q_{11}} |e_{11}|^{\frac{p_{11}}{q_{11}}-1} e_{12}) - \hat{\delta}_\psi\end{aligned}\quad (54)$$

where $\hat{\delta}_\phi, \hat{\delta}_\theta, \hat{\delta}_\psi$ are the compensated saturation errors. To ensure that the arrival phase of the sliding mode has the same dynamic quality as the movement phase of the sliding mode surface, we adopt a reaching law which is given as:

$$\dot{\sigma}_v = -\varphi_v \sigma_v - \gamma_v \sigma_v^{\frac{m_v}{n_v}} \quad (v = \phi, \theta, \psi) \quad (55)$$

where $\gamma_v = \frac{L_{v0} + L_{v1}|v| + L_{v2}|\dot{v}|}{m_v} + \eta_v$, $\varphi_v > 0$, $\eta_v > 0$, m_v, n_v ($m_v < n_v$) are $|\sigma_v|$ positive odd constants, $L_{v0} + L_{v1}|v| + L_{v2}|\dot{v}|$ is the upper bound of disturbances and uncertainty, L_{v0}, L_{v1}, L_{v2} are unknown positive constants.

Hence, the switching control laws in attitude systems are provided as:

$$\begin{aligned} U_{sw2}^* &= -\frac{1}{w_1} \left(\varphi_\phi \sigma_\phi + \left(\frac{\hat{L}_{\phi 0} + \hat{L}_{\phi 1} |\phi| + \hat{L}_{\phi 2} |\dot{\phi}|}{|\sigma_\phi^{\frac{m_\phi}{n_\phi}}|} + \eta_\phi \right) \sigma_\phi^{\frac{m_\phi}{n_\phi}} \right) \\ U_{sw3}^* &= -\frac{1}{w_2} \left(\varphi_\theta \sigma_\theta + \left(\frac{\hat{L}_{\theta 0} + \hat{L}_{\theta 1} |\theta| + \hat{L}_{\theta 2} |\dot{\theta}|}{|\sigma_\theta^{\frac{m_\theta}{n_\theta}}|} + \eta_\theta \right) \sigma_\theta^{\frac{m_\theta}{n_\theta}} \right) \\ U_{sw4}^* &= -\frac{1}{w_3} \left(\varphi_\psi \sigma_\psi + \left(\frac{\hat{L}_{\psi 0} + \hat{L}_{\psi 1} |\psi| + \hat{L}_{\psi 2} |\dot{\psi}|}{|\sigma_\psi^{\frac{m_\psi}{n_\psi}}|} + \eta_\psi \right) \sigma_\psi^{\frac{m_\psi}{n_\psi}} \right) \end{aligned} \quad (56)$$

where $\hat{L}_{v0}, \hat{L}_{v1}, \hat{L}_{v2}$ are adaptive values.

According to the analysis of Remark 4, we directly give the result of the adaptive laws of attitude loop here:

$$\dot{L}_{v0} = \begin{cases} \mu_{v0} |\sigma_v|, & \text{for } |\sigma_v| \geq \varepsilon \\ 0, & \text{for } |\sigma_v| < \varepsilon \end{cases} \quad (57)$$

$$\dot{L}_{v1} = \begin{cases} \mu_{v1} |\sigma_v| |v|, & \text{for } |\sigma_v| \geq \varepsilon \\ 0, & \text{for } |\sigma_v| < \varepsilon \end{cases} \quad (58)$$

$$\dot{L}_{v2} = \begin{cases} \mu_{v2} |\sigma_v| |\dot{v}|, & \text{for } |\sigma_v| \geq \varepsilon \\ 0, & \text{for } |\sigma_v| < \varepsilon \end{cases} \quad (59)$$

where $\mu_{v0}, \mu_{v1}, \mu_{v2} > 0 (v = \phi, \theta, \psi)$.

The attitude control laws can be written as:

$$\begin{cases} U_2^* = \frac{1}{w_1} (k_4 w_1 h_8 + \ddot{\phi}_d - q_1 h_{10} h_{12} - \alpha_7 e_8 \\ \quad - \beta_7 \frac{p_7}{q_7} |e_7|^{\frac{p_7}{q_7}-1} e_8 - \varphi_\phi \sigma_\phi - \gamma_\phi \sigma_\phi^{\frac{m_\phi}{n_\phi}}) - \hat{\delta}_\phi \\ U_3^* = \frac{1}{w_2} (k_5 w_2 h_{10} + \ddot{\theta}_d - q_2 h_8 h_{12} - \alpha_9 e_{10} \\ \quad - \beta_9 \frac{p_9}{q_9} |e_9|^{\frac{p_9}{q_9}-1} e_{10} - \varphi_\theta \sigma_\theta - \gamma_\theta \sigma_\theta^{\frac{m_\theta}{n_\theta}}) - \hat{\delta}_\theta \\ U_4^* = \frac{1}{w_3} (k_6 w_3 h_{12} + \ddot{\psi}_d - q_3 h_8 h_{10} - \alpha_{11} e_{12} \\ \quad - \beta_{11} \frac{p_{11}}{q_{11}} |e_{11}|^{\frac{p_{11}}{q_{11}}-1} e_{12} - \varphi_\psi \sigma_\psi - \gamma_\psi \sigma_\psi^{\frac{m_\psi}{n_\psi}}) - \hat{\delta}_\psi \end{cases} \quad (60)$$

Theorem 3. Considering the ϕ -subsystem (6) with the surface (52) and the anti-saturation auxiliary compensator (15). The controllers and the adaptive laws are designed as (60) and (57)–(59). The system is uniformly bounded stable and σ_ϕ converges asymptotically to 0, then the following statements hold:

- (i) The error e_7 converges to zero in a finite time;
- (ii) All signals of the ϕ -subsystem (6) are bounded.

Proof. A Lyapunov function is selected as follows:

$$V_\phi = \frac{1}{2} \sigma_\phi^2 + \frac{1}{2} \hat{\delta}_\phi^2 + \frac{1}{2\mu_{\phi i}} \sum_{i=0}^2 \tilde{L}_{\phi i}^2 \quad (61)$$

where $\mu_{\phi i}$ is positive number and $\tilde{L}_{\phi i} = \hat{L}_{\phi i} - L_{\phi i} (i = 0, 1, 2)$.

The derivative of V_ϕ is:

$$\dot{V}_\phi = \sigma_\phi \dot{\sigma}_\phi + \hat{\delta}_\phi \dot{\hat{\delta}}_\phi + \frac{1}{\mu_{\phi i}} \sum_{i=0}^2 \tilde{L}_{\phi i} \dot{\tilde{L}}_{\phi i} \quad (62)$$

Substituting the equation (15) into equation (62), we can obtain:

$$\begin{aligned} \dot{V}_\phi &= \sigma_\phi \left(w_1 \delta_\phi - w_1 \hat{\delta}_\phi + d_\phi - \varphi_\phi \sigma_\phi - \gamma_\phi \sigma_\phi^{\frac{m_\phi}{n_\phi}} \right) \\ &\quad + \hat{\delta}_\phi \left(-\bar{c}_\phi \hat{\delta}_\phi + w_1 \sigma_\phi - \frac{|w_1 \sigma_\phi \delta_\phi| + \frac{1}{2} \hat{\delta}_\phi^2}{|\hat{\delta}_\phi|^2} \hat{\delta}_\phi + \delta_\phi \right) \\ &\quad + \frac{1}{\mu_{\phi i}} \sum_{i=0}^2 \tilde{L}_{\phi i} \dot{\tilde{L}}_{\phi i} \\ &= \sigma_\phi \left(-\varphi_\phi \sigma_\phi - \left(\frac{\hat{L}_{\phi 0} + \hat{L}_{\phi 1} |\phi| + \hat{L}_{\phi 2} |\dot{\phi}|}{|\sigma_\phi^{\frac{m_\phi}{n_\phi}}|} + \eta_\phi \right) \sigma_\phi^{\frac{m_\phi}{n_\phi}} + d_\phi \right) \\ &\quad + w_1 \sigma_\phi \delta_\phi - \bar{c}_\phi \hat{\delta}_\phi^2 + \hat{\delta}_\phi \delta_\phi - |w_1 \sigma_\phi \delta_\phi| \\ &\quad - \frac{1}{2} \hat{\delta}_\phi^2 + \frac{1}{\mu_{\phi i}} \sum_{i=0}^2 (\hat{L}_{\phi i} - L_{\phi i}) \dot{\tilde{L}}_{\phi i} \end{aligned} \quad (63)$$

Substituting the equations (57)–(59) into equation (63), then we get:

$$\begin{aligned} \dot{V}_\phi &= \sigma_\phi \left(-\varphi_\phi \sigma_\phi - \left(\frac{\hat{L}_{\phi 0} + \hat{L}_{\phi 1} |\phi| + \hat{L}_{\phi 2} |\dot{\phi}|}{|\sigma_\phi^{\frac{m_\phi}{n_\phi}}|} + \eta_\phi \right) \sigma_\phi^{\frac{m_\phi}{n_\phi}} + d_\phi \right) \\ &\quad + \frac{1}{\mu_{\phi 0}} (\hat{L}_{\phi 0} - L_{\phi 0}) \mu_{\phi 0} |\sigma_\phi| \\ &\quad + \frac{1}{\mu_{\phi 1}} (\hat{L}_{\phi 1} - L_{\phi 1}) \mu_{\phi 1} |\phi| |\sigma_\phi| \\ &\quad + \frac{1}{\mu_{\phi 2}} (\hat{L}_{\phi 2} - L_{\phi 2}) \mu_{\phi 2} |\dot{\phi}| |\sigma_\phi| \\ &\quad + w_1 \sigma_\phi \delta_\phi - |w_1 \sigma_\phi \delta_\phi| - \bar{c}_\phi \hat{\delta}_\phi^2 + \hat{\delta}_\phi \delta_\phi - \frac{1}{2} \hat{\delta}_\phi^2 \end{aligned} \quad (64)$$

Because of equation (43), we can get:

$$\begin{aligned} \dot{V}_\phi &\leq \sigma_\phi [-\varphi_\phi \sigma_\phi - \left(\frac{L_{\phi 0} + L_{\phi 1} |v| + L_{\phi 2} |\dot{v}|}{|\sigma_\phi^{\frac{m_\phi}{n_\phi}}|} + \eta_\phi - \frac{d_\phi}{\sigma_\phi^{\frac{m_\phi}{n_\phi}}} \right) \sigma_\phi^{\frac{m_\phi}{n_\phi}}] - \left(\bar{c}_\phi - \frac{1}{2} \right) \hat{\delta}_\phi^2 \end{aligned} \quad (65)$$

where $\bar{c}_\phi > \frac{1}{2}$. Because of $\gamma_\phi > \frac{d_\phi}{\sigma_\phi^{\frac{m_\phi}{n_\phi}}}$, we can obtain $\gamma_\phi^{**} > 0$, then we get:

$$\dot{V}_\phi \leq -(\varphi_\phi \sigma_\phi^2 + \gamma_\phi^\star \sigma_\phi^{\frac{m_\phi+n_\phi}{n_\phi}}) \leq 0 \quad (66)$$

where $(m_\phi + n_\phi)$ is an even number. Obviously, V_ϕ is positive definite and lower bounded, \dot{V}_ϕ is negative semi-definite. In the initial condition $V_\phi(t) \leq V_\phi(0)$, V_ϕ is bounded, so e_7 , $\tilde{L}_{\phi i}$, σ_ϕ and $\hat{\delta}_\phi$ are proved to be bounded when $t \rightarrow \infty$, then we can conclude U_2^* and δ_ϕ are bounded. $\sigma_\phi \neq 0$, $\dot{V}_\phi < 0$. So $t \rightarrow \infty$, $\sigma_\phi \rightarrow 0$, $\dot{V}_\phi \rightarrow 0$. When $\sigma_\phi = 0$, $\dot{V}_\phi = 0$, $\tilde{L}_{\phi i}$ and $\hat{\delta}_\phi$ keep static. In summary, we obtain that σ_ϕ converges asymptotically to 0, the ϕ -system is uniformly bounded stable and all signals are eventually bounded. Furthermore, we give an analysis for sliding mode arrival time. Base on equation (55), we can get:

$$\sigma_\phi^{\frac{m_\phi}{n_\phi}} \frac{d\sigma_\phi}{dt} + \varphi_\phi \sigma_\phi^{1-\frac{m_\phi}{n_\phi}} = -\gamma_\phi \quad (67)$$

let $s = \sigma_\phi^{\frac{1-m_\phi}{n_\phi}}$, and $\frac{ds}{dt} = \frac{n_\phi - m_\phi}{n_\phi} \sigma_\phi^{\frac{-m_\phi}{n_\phi}} \frac{d\sigma_\phi}{dt}$, equation (67) can be expressed as:

$$\frac{ds}{dt} + \frac{n_\phi - m_\phi}{n_\phi} \varphi_\phi s = -\frac{n_\phi - m_\phi}{n_\phi} \gamma_\phi \quad (68)$$

The solution of equation (68) is:

$$s = e^{-\int_0^{t_n} \frac{n_\phi - m_\phi}{n_\phi} \varphi_\phi dt} \left(- \int_0^t \frac{n_\phi - m_\phi}{n_\phi} \gamma_\phi e^{\frac{n_\phi - m_\phi}{n_\phi} \varphi_\phi t} dt + C \right) \quad (69)$$

Based on equation (69), the convergence time of the sliding mode arrival phase is:

$$t_r = \frac{n_\phi}{\varphi_\phi(n - m_\phi)} \ln \frac{\gamma_\phi + \varphi_\phi \sigma_\phi(0)^{\frac{n_\phi - m_\phi}{n_\phi}}}{\gamma_\phi} \quad (70)$$

When the system is on $\sigma_\phi = 0$, for the system $\dot{e}_7 = -\alpha_7 e_7 - \beta_7 |e_7|^{\frac{p_7}{q_7}} \text{sign}(e_7)$, define the Lyapunov function $V'_\phi = \frac{1}{2} e_7^2$, we have:

$$\begin{aligned} \dot{V}'_\phi &= e_7 \dot{e}_7 \\ &= -\alpha_7 e_7^2 - \beta_7 |e_7|^{\frac{p_7}{q_7} + 1} \\ &\leq -(\alpha_7 |e_7| + \beta_7 |e_7|^{\frac{p_7}{q_7}}) \sqrt{2} \frac{|e_7|}{\sqrt{2}} \\ &= -\sqrt{2} \zeta' V'_\phi(t) \end{aligned} \quad (71)$$

where $\zeta' = \alpha_7 |e_7| + \beta_7 |e_7|^{\frac{p_7}{q_7}}$. According to the Lemma 2, e_7 converges to zero in the finite time is:

$$t_a \leq \frac{\sqrt{2 V'_\phi(0)}}{\zeta'} \quad (72)$$

Finally, the ϕ -system uniformly bounded stability is ensured and all signals of ϕ -system are bounded. The θ -system, ψ -system are uniformly bounded stable by

using similar proof methods and the process is omitted here for the save of space. This completes the proof.

Theorem 4. The attitude subsystem is uniformly bounded stable under the controllers U_2^* , U_3^* , and U_4^* .

Proof. A Lyapunov function is defined as follows:

$$\begin{aligned} V_a &= V_\phi + V_\theta + V_\psi \\ &= \frac{1}{2} \sigma_\phi^2 + \frac{1}{2} \hat{\delta}_\phi^2 + \frac{1}{2\mu_{\phi i}} \sum_{i=0}^2 \tilde{L}_{\phi i}^2 + \frac{1}{2} \sigma_\theta^2 + \frac{1}{2} \hat{\delta}_\theta^2 \\ &\quad + \frac{1}{2\mu_{\theta i}} \sum_{i=0}^2 \tilde{L}_{\theta i}^2 + \frac{1}{2} \sigma_\psi^2 + \frac{1}{2} \hat{\delta}_\psi^2 + \frac{1}{2\mu_{\psi i}} \sum_{i=0}^2 \tilde{L}_{\psi i}^2 \end{aligned} \quad (73)$$

The derivative of V_a is:

$$\begin{aligned} \dot{V}_a &= \sigma_\phi \dot{\sigma}_\phi + \hat{\delta}_\phi \dot{\hat{\delta}}_\phi + \frac{1}{\mu_{\phi i}} \sum_{i=0}^2 \tilde{L}_{\phi i} \dot{\tilde{L}}_{\phi i} + \sigma_\theta \dot{\sigma}_\theta + \hat{\delta}_\theta \dot{\hat{\delta}}_\theta \\ &\quad + \frac{1}{\mu_{\theta i}} \sum_{i=0}^2 \tilde{L}_{\theta i} \dot{\tilde{L}}_{\theta i} + \sigma_\psi \dot{\sigma}_\psi + \hat{\delta}_\psi \dot{\hat{\delta}}_\psi + \frac{1}{\mu_{\psi i}} \sum_{i=0}^2 \tilde{L}_{\psi i} \dot{\tilde{L}}_{\psi i} \end{aligned} \quad (74)$$

Simplifying above equation and replacing the (15), (60) into equation (74), it yields:

$$\begin{aligned} \dot{V}_a &\leq -(\varphi_\phi \sigma_\phi^2 + \gamma_\phi^\star \sigma_\phi^{\frac{m_\phi+n_\phi}{n_\phi}}) - (\varphi_\theta \sigma_\theta^2 + \gamma_\theta^\star \sigma_\theta^{\frac{m_\theta+n_\theta}{n_\theta}}) \\ &\quad - (\varphi_\psi \sigma_\psi^2 + \gamma_\psi^\star \sigma_\psi^{\frac{m_\psi+n_\psi}{n_\psi}}) \leq 0 \end{aligned} \quad (75)$$

From the previous analysis, it follows that the attitude subsystem is uniformly bounded stable. Finally, both the position and attitude loops of the quadrotor are proven stable by Lyapunov direct method, that is, the whole closed-loop control system is stable and effective.

Simulation results

In this work, the proposed NDOB-AFNNTSM scheme is tested in the Simulink for the quadrotor tracking problem. The Simulink chooses a fixed step of 0.009 with the fourth-order Runge-Kutta algorithm. Moreover, unmodeled dynamics such as 30% random variation in moment of inertia is considered. We purposely compare it with four approaches. These four methods are PID,²⁴ NTSMC, TSMC, fuzzy gains terminal sliding mode control (FGTSMC).^{25,26} Consider the physical parameters of the quadrotor used in simulation as: $m = 1.5 \text{ Kg}$, $l = 0.225 \text{ m}$, $g = 9.8 \text{ m/s}^2$, $J_{xx} = 0.0211 \text{ Kg} \cdot \text{m}^2$, $J_{yy} = 0.0212 \text{ Kg} \cdot \text{m}^2$, $J_{zz} = 0.0366 \text{ Kg} \cdot \text{m}^2$, $k_1 = k_2 = k_3 = 0.01 \text{ N} \cdot \text{s/m}$, $k_4 = k_5 = k_6 = 0.01 \text{ N} \cdot \text{s/rad}$.

Consider the parameters of the controller as: $\epsilon = 5$, $\bar{c}_v = 2$, $\hat{\delta}_{vr} = 0.001$, $c_1 = c_3 = c_5 = 1.5$, $\alpha_1 = \alpha_3 = \alpha_5 = 2.5$, $\beta_1 = \beta_3 = \beta_5 = 0.1$, $\lambda_{1x} = \lambda_{1y} = \lambda_{2x} = \lambda_{2y} = 0.01$, $\lambda_{1z} = \lambda_{2z} = 0.1$, $b_x = b_y = b_z = 1.1$, $\mu_v = 0.01$, $\alpha_7 = \alpha_9 = \alpha_{11} = 2$, $\beta_7 = \beta_9 = \beta_{11} = 1$, $p_i = 9$, $q_i = 5$, $\eta_\psi = \varphi_\phi = \varphi_\theta = 15$, $\varphi_\psi = 75$, $n_v = 5$, $m_v = 3$, $\eta_x = \eta_y = \eta_z = 2.5$, $\mu_{v0} = \mu_{v1} = \mu_{v2} = \eta_\phi = \eta_\theta = 0.1$.

Controller parameter tuning rules

In reality, quadrotor tracking performance and controller effectiveness are affected by system inertia, actuator saturation, or sensor noise. Due to the practical double closed-loop system, the dynamic performance of the inner-loop affects the stability of the outer-loop, which in turn plays a critical role in the overall closed-loop system. In order to ensure fast and stable convergence of the closed loop, engineering generally requires the inner-loop to respond faster than the outer-loop. This requires that the controllers gain of the inner-loop are larger than or at least similar to those of the outer-loop. There is no necessary relationship between the parameter settings of the different degrees of freedom of in outer-loop, and the same applies to the inner-loop. For convenience a consistent parameter magnitude can be chosen in each loop. However, since the actuator saturation is considered in this paper, the controller parameters with a large degree of limitation can be chosen smaller to reduce the saturation phenomenon. Based on the above principles, we give some parameter adjustment details:

- (i) Selection of parameter in sliding mode surfaces: The parameter $\alpha_i, \beta_i, c_i (i = 1, 3, 5)$ in (27) is designed to regulate the convergence time when $\sigma_v = 0 (v = x, y, z)$. α_i determines the speed of convergence of the linear term, and α_i guarantee the rapidity when the error is far from zero. Increasing β_i and c_i allows the system to converge quickly as it approaches the origin. Excessive α_i and β_i increase the controller amplitude. An excessive c_i makes the system slower near zero, but reduces steady-state chattering. Adjustment of these parameters requires a combination of consideration, and selecting a set of suitable parameters after multiple adjustments. Similarly, the parameter in (52) are adjusted in the same way, but make sure that the attitude loop parameters are larger than or at least similar to those of the position loop.
- (ii) Selection of parameter in switching control: The parameter $\lambda_{1v}, \lambda_{2v}, \eta_v (v = x, y, z)$ in (32) is designed to adjust the reaching speed when $\sigma_v \rightarrow 0 (v = x, y, z)$. $b_v > 1$ is selected to meet that $b_v^{|\sigma_v|} - 1$ is positive. Not larger $\lambda_{1v}, \lambda_{2v}$ will increase the response speed but not cause chattering. η_v should not be too small because it will reduce the robustness at steady state. The

parameter $\varphi_v, \eta_v, \frac{m_v}{n_v} (v = \phi, \theta, \psi)$ in (56) is designed to adjust the reaching speed when $\sigma_v \rightarrow 0 (v = \phi, \theta, \psi)$. Choosing large enough $\eta_v, \frac{m_v}{n_v}$ can make the convergence field of the sliding mode vector smaller, but it also increases the chattering in this field. Increasing φ_v improves the response speed when σ_v is far from 0. φ_v needs to be large enough to ensure that the inner-loop is faster than the outer-loop.

- (iii) Selection of adaptive parameters: The adaptive gains in (34), (57)–(59), can be chosen not too large, both to ensure fast convergence and not to overestimate, but too large gains may aggravate the actuator saturation.

Remark 5. The parameters of the quadrotor are selected from <https://www.flyeval.com/>, and the maximum thrust of the selected DJI quadrotor is 26.55 N. The control input is allocated according to the maximum thrust and channels priority. Torque input is similar to duty cycle from -1 to 1. Based on the control allocation of each channel, we set the following constraints on the inputs:

$$\begin{aligned} |U_x| &\leq 2 \text{ N}, |U_y| \leq 2 \text{ N}, |U_z| \leq 7 \text{ N}, U_1 \leq 26.55 \text{ N} \\ |U_2| &\leq 1 \text{ N} \cdot \text{m}, |U_3| \leq 1 \text{ N} \cdot \text{m}, |U_4| \leq 1 \text{ N} \cdot \text{m} \end{aligned} \quad (76)$$

Scenario 1

In this case, we provide a novel 3-D desired trajectory for quadrotor as follows:

$$\begin{aligned} x_d &= \begin{cases} 2 \text{ m}, t \in [0, 2\pi] \\ \sin(t) + 2 \text{ m}, t \in [2\pi, 40] \end{cases} \\ y_d &= \begin{cases} 2 \text{ m}, t \in [0, 2\pi] \\ \cos(t) + 1 \text{ m}, t \in [2\pi, 40] \end{cases} \\ z_d &= \begin{cases} 2 \text{ m}, t \in [0, 2\pi] \\ 1 + \cos^2(t) + 2 \sin^2(t) \text{ m}, t \in [2\pi, 40] \end{cases} \\ \psi_d &= 30^\circ, t \in [0, 40] \end{aligned} \quad (77)$$

The disturbances are described as follows:

$$\begin{aligned} d_x &= 0.8 \cos(t) \text{ m/s}^2, d_\phi = 0.5 \sin(t) \text{ rad/s}^2, \\ d_y &= 0.8 \sin(\frac{\pi t}{3}) \text{ m/s}^2, d_\theta = 0.5 \sin(t) \text{ rad/s}^2, \\ d_z &= 0.8 \sin(t) \text{ m/s}^2, d_\psi = 0.5 \sin(t) \text{ rad/s}^2 \end{aligned} \quad (78)$$

Figure 4(a) shows the results of 3D trajectory tracking. Figure 4(b) suggests the favorable effect of the NDOB, which gives compensation for unknown disturbances. From Figure 5(a), the position tracking has few errors, while several of the compared methods have certain steady-state errors from beginning to end. In addition, Figure 5(b) shows that the tracking process of attitude angle does not perform drastic

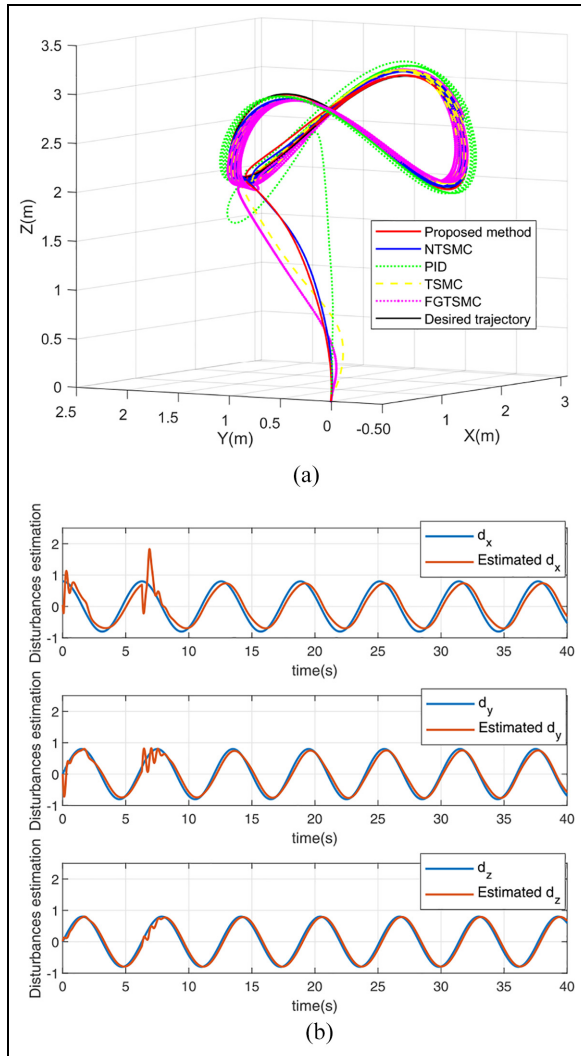


Figure 4. Tracking and disturbances in Scenario 1: (a) 3-D tracking and (b) observed disturbances.

changes, indicating that the quadrotor is in a stable flight process.

Figure 6(a) shows that the control inputs are limited to the specified range. U_2 and U_3 have short transient response times in the beginning, and then the curves become stable. Using $\tanh(\cdot)$ instead of $\text{sign}(\cdot)$ can enhance the smoothness of the control curve. Figure 6(b) provides a set of comparisons. The results illustrate the remarkable effect of using the method in this paper for chattering suppression. The control curve of the proposed method is smooth and does not have excessive gain. In contrast, the compared methods are much worse. Figure 7(a) and (b) show the effect of the estimation of the saturated error, it can be seen that the compensated value and actual value are bounded. In Figure 7(c), it can be observed that the curve of the unknown upper bound of the estimated NDOB errors. The curve finally remains stable, indicating that the adaptive value is no longer growing. Similarly, we can obtain the same conclusion in Figure 7(d), where the adaptive value of the

attitude loop also remains stable, suggesting that the dead zone method is feasible.

Scenario 2

In the scenario 2, the simulation is implemented with a square 3-D trajectory. The ideal trajectory is shown in Table 1. The disturbances are described as equation (79):

$$\begin{aligned}
 d_x &= \begin{cases} 0.27 \sin(t-1) + 0.46 \cos\left(\frac{\pi}{3}t\right) \text{ m/s}^2, t \in [0, 10] \\ 0.77 \text{ m/s}^2, t \in [10, 20] \\ 0.52 \sin\left(\frac{5t}{7}-0.7\right) \text{ m/s}^2, t \in [20, 60] \\ 0.7 \text{ m/s}^2, t \in [60, 70] \end{cases} \\
 d_y &= \begin{cases} 0.45 \sin\left(\frac{\pi}{3}t\right) + 0.27 \cos(t-2.1) \text{ m/s}^2, t \in [0, 10] \\ -0.77 \text{ m/s}^2, t \in [10, 20] \\ 0.58 \cos\left(\frac{3t}{4}+1.2\right) \text{ m/s}^2, t \in [20, 60] \\ -0.7 \text{ m/s}^2, t \in [60, 70] \end{cases} \\
 d_z &= \begin{cases} 0.47 \cos\left(\frac{\pi}{3}t\right) + 0.25 \sin(1.55t-10\pi) \text{ m/s}^2, t \in [0, 10] \\ 0.82 \text{ m/s}^2, t \in [10, 20] \\ 0.7 \sin(t+\frac{\pi}{4}) \text{ m/s}^2, t \in [20, 60] \\ 0.75 \text{ m/s}^2, t \in [60, 70] \end{cases} \\
 d_\phi &= \begin{cases} 0.5 \cos(0.2t) \text{ rad/s}^2, t \in [0, 10] \\ 0.5 \text{ rad/s}^2, t \in [10, 20] \\ 0.5 \sin(t) \text{ rad/s}^2, t \in [20, 60] \\ 0.5 \text{ rad/s}^2, t \in [60, 70] \end{cases} \\
 d_\theta &= \begin{cases} 0.5 \sin(0.2t) \text{ rad/s}^2, t \in [0, 10] \\ 0.5 \text{ rad/s}^2, t \in [10, 20] \\ 0.5 \sin(t) \text{ rad/s}^2, t \in [20, 60] \\ 0.5 \text{ rad/s}^2, t \in [60, 70] \end{cases} \\
 d_\psi &= \begin{cases} 0.5 \cos(0.2t) \text{ rad/s}^2, t \in [0, 10] \\ 0.5 \text{ rad/s}^2, t \in [10, 20] \\ 0.5 \sin(t) \text{ rad/s}^2, t \in [20, 60] \\ 0.5 \text{ rad/s}^2, t \in [60, 70] \end{cases}
 \end{aligned} \tag{79}$$

Figure 8(a) shows the quadrotor as a square motion in the specified path. The results of observed disturbances is given in Figure 8(b). In Figure 9(a), it can be derived that there is a faster response than other methods when the specified trajectory changes abruptly, and the control accuracy remains good. Figure 9(b) shows that the change of attitude. There is a small tracking error, and the whole process is relatively smooth. In Figure 10(a), the square trajectory has several inflection points, but the chattering is not too dramatic. From Figure 10(b) it can be seen that the compared methods have dramatic chattering.

Finally, two set of comparison tests for performance indexes is applied to evaluate the distinction between the proposed NDOB-AFNTSM method and PID, NTSMC, TSMC, FGSMC. The error squared integration (ESI) can be described as follows:

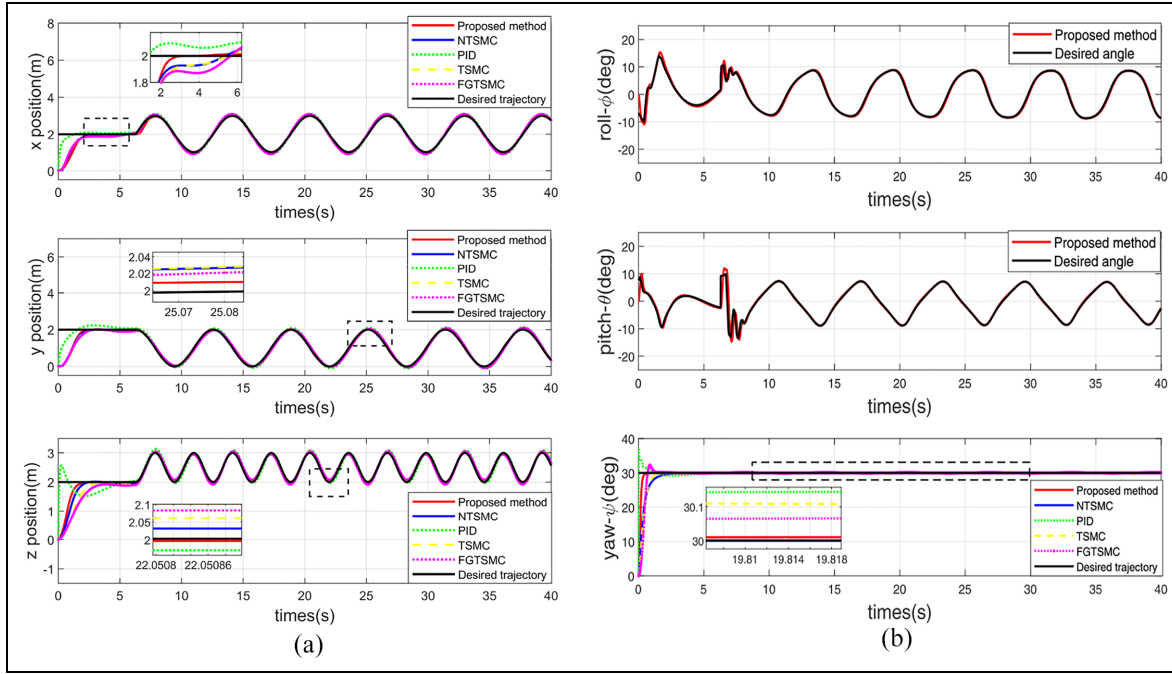


Figure 5. Tracking performance in Scenario I: (a) position tracking and (b) attitude tracking.

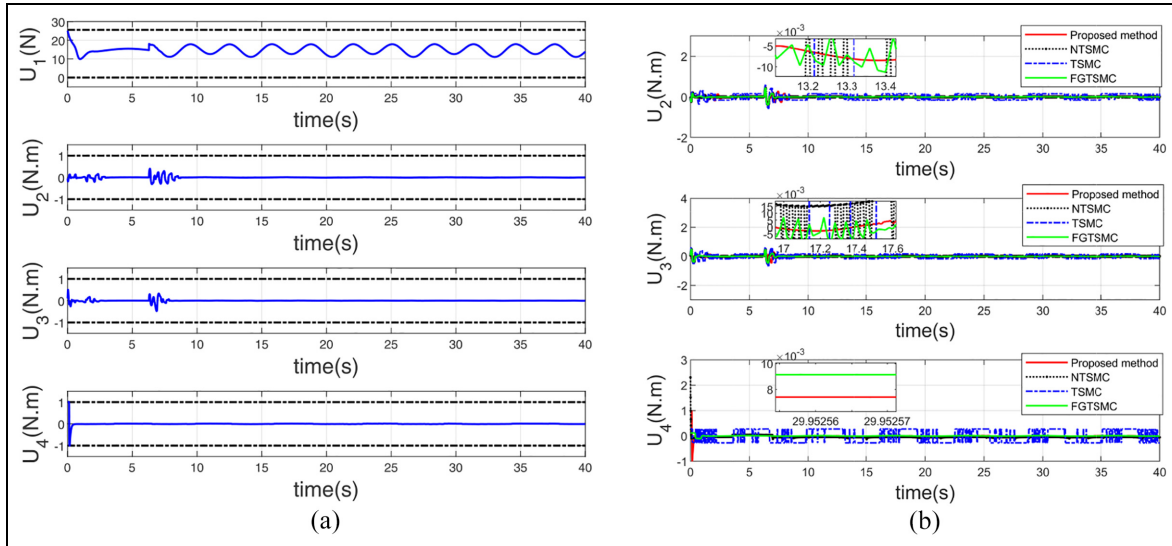


Figure 6. Control inputs in Scenario I: (a) control inputs and (b) control inputs comparison.

$$\text{ESI} = \int_{t_0}^{t_s} e^2 dt \quad (80)$$

where t_0 is the initial time of the simulation, t_s presents final time, e is track error.

Remark 6. Different controllers are affected differently by the initial transient. We compare the ESI in the steady-state tracking period for a fair comparison. The initial transient time is chosen to be 2 s. In particular, the trajectory changes of scenes 1 and 2 are piecewise. It is meaningful to exclude the initial

transient at each stage. In the Tables 2 and 3 respecting to performance indexes, the best results are shown in bold text.

It is shown in Table 2 that the proposed idea guarantees a high accuracy compared with other methods among two scenarios. Although some attitude angles tracking of the PID works well, it is almost the same as the proposed method. The proposed method generally outperforms other similar methods under complex disturbances and trajectories with abnormal changes. It is worth noting that the other methods do not consider actuator saturation. This indicates that

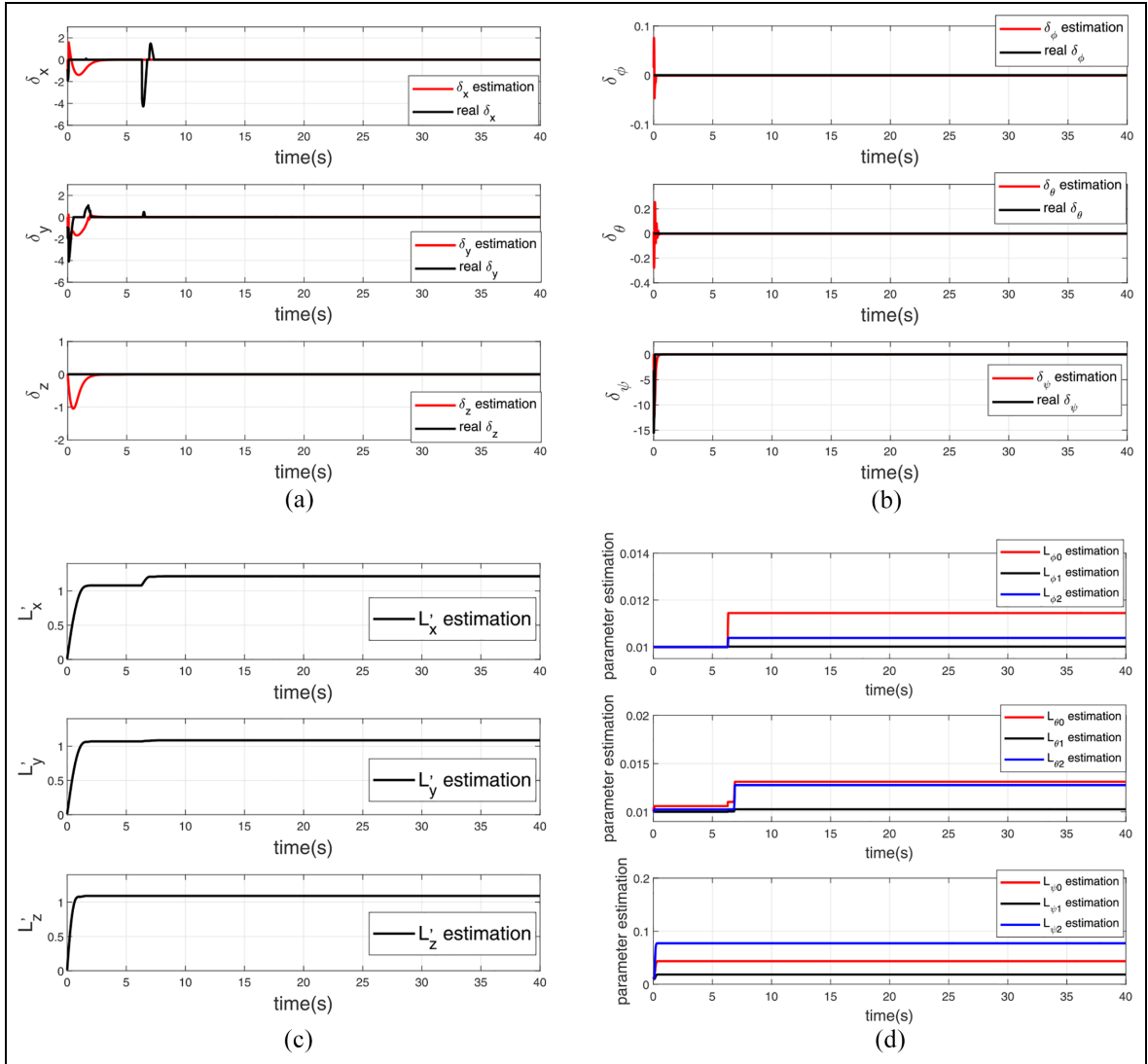


Figure 7. Adaptive results in Scenario I: (a) saturation errors for position, (b) saturation errors for attitude, (c) parameter estimation for position, and (d) parameter estimation for attitude.

Table I. Square 3D trajectory.

Desired path	Value	Time(s)
$[x_d(m), y_d(m), z_d(m)]$	$[1, 1, 3]$	$[0, 10]$
	$[3, 1, 3]$	$(10, 20]$
	$[3, 3, 3]$	$(20, 30]$
	$[1, 3, 3]$	$(30, 40]$
	$[1, 1, 3]$	$(40, 70]$
$\psi_d(\text{deg})$	15°	$[0, 70]$

the results of the proposed method is meaningful. On the other hand, the IAU and the IADU are used to evaluate the controller signals, they can be described as:

$$\text{IAU} = \int_{t_0}^{t_s} |u(t)| dt, \quad \text{IADU} = \int_{t_0}^{t_s} \left| \frac{du(t)}{dt} \right| dt \quad (81)$$

where t_0 is the initial time of the simulation, t_s presents final time, $u(t)$ is the control input.

The IAU is a standard for describing the magnitude of the signal amplitude. The purpose of the IADU is to detect the smoothness of the signals. The IADU becomes more smaller, the anti-chattering ability of signals becomes more stronger. As seen in Table 3, the control signal generated by the proposed NDOB-AFNTSM method has an excellent anti-chattering capability. FGTSMC has a better ability to suppress chattering for u_4 than NDOB-AFNTSM, but the IADU value of NDOB-AFNTSM is also minimal. Lastly, the signal amplitude is tiny without excessive energy consumption. This means that the adaptive anti-saturation technique ensures that the control gain is limited to a small range.

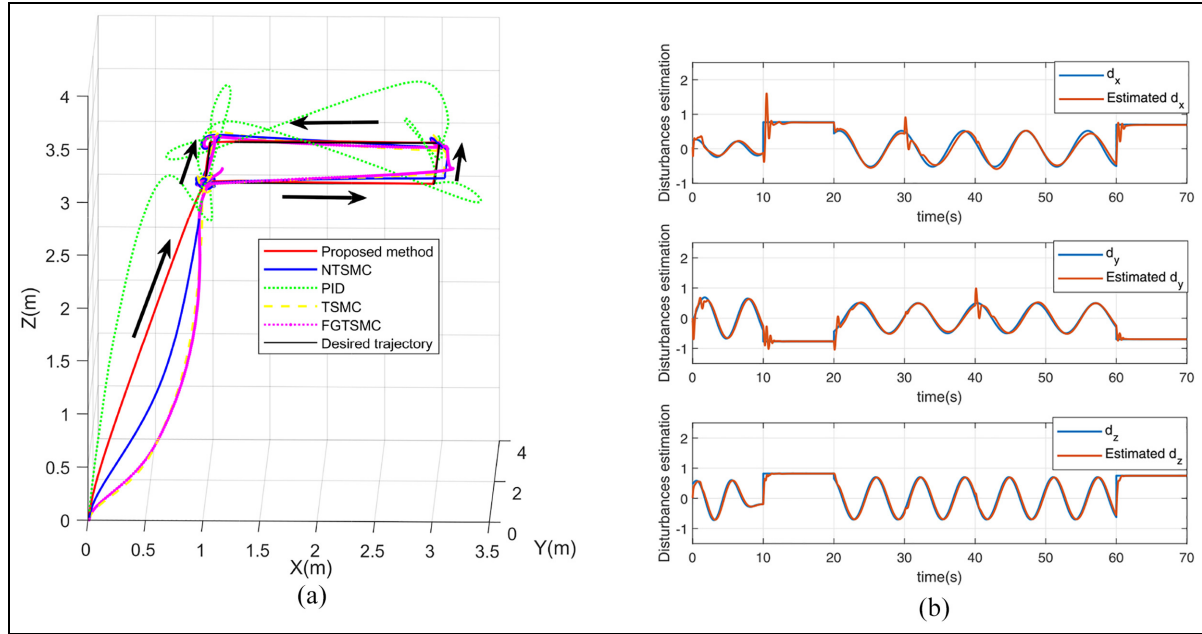


Figure 8. Tracking and disturbances in Scenario 2: (a) 3-D tracking and (b) observed disturbances.

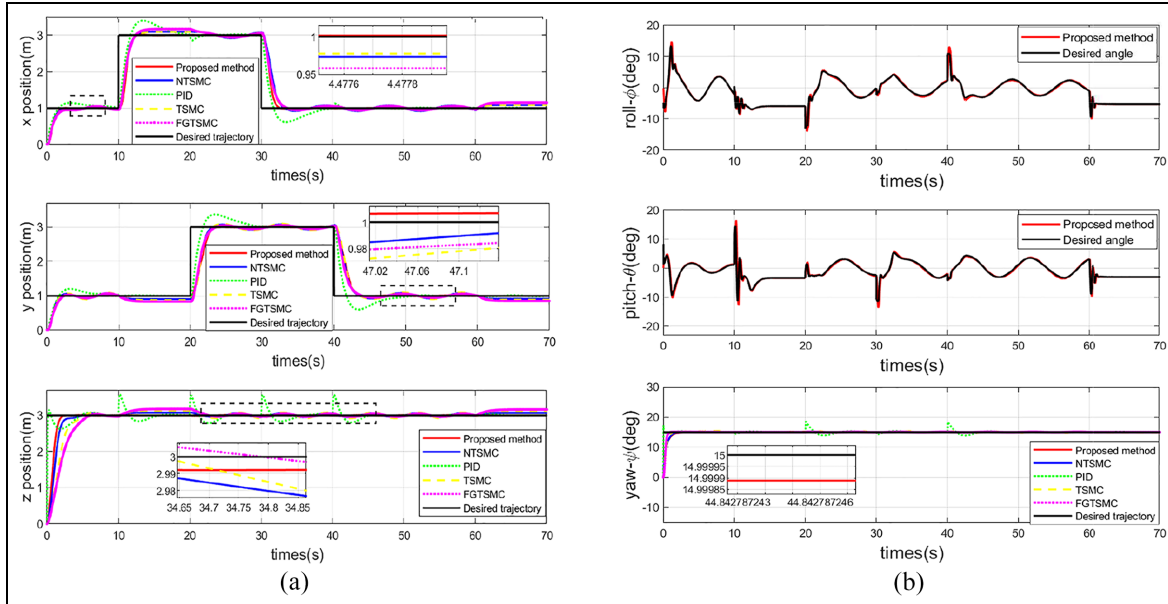


Figure 9. Tracking performance in Scenario 2: (a) position tracking and (b) attitude tracking.

Conclusion

This paper establishes a quadrotor dynamics model based on the Newton-Euler equation. The double closed-loop NDOB-AFNNTSM controller is adopted to address the tracking control problem of a quadrotor with unknown disturbances, unmodeled dynamics and actuator saturation. The proposed method avoids the singularity problem of TSMC. The complex disturbances are compensated for position outer-loop. The adaptive law estimates the unknown bounds of the NDOB errors in the position

subsystem and the uncertainty in the attitude subsystem. Dead zone method effectively solves the over-estimation problem. Furthermore, the anti-saturation auxiliary compensator estimates unknown saturation errors, which fixes the problem of actuator saturation. The proposed method has good robustness and can achieve accurate tracking under complex disturbances. Simulation results show the improved convergence speed and accuracy using the proposed scheme. Finally, the strength of the proposed NDOB-AFNNTSM scheme is illustrated by comparative studies for performance indexes in simulation.

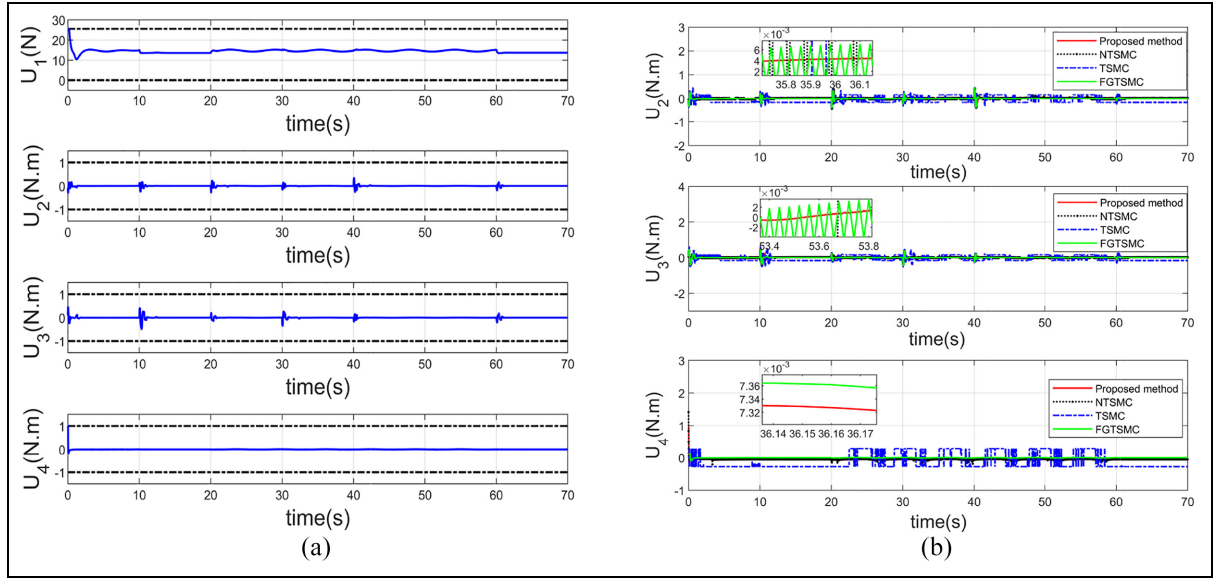


Figure 10. Control inputs in Scenario 2: (a) control inputs and (b) control inputs comparison.

Table 2. ESI indexes.

State	Proposed NDOB-AFNTSM	NTSMC	PID	TSMC	FGTSMC
Scenario 1					
x	0.0135	0.0332	0.0736	0.0331	0.0418
y	0.0038	0.0427	0.0825	0.0511	0.0794
z	0.0017	0.0264	0.0718	0.0347	0.0619
ϕ	0.0054	0.0116	0.0086	0.0192	0.0093
θ	0.0103	0.0204	0.0411	0.0279	0.0363
ψ	0.0002	0.0006	0.0001	0.0013	0.0007
Scenario 2					
x	0.0142	0.0486	0.0829	0.0514	0.0602
y	0.0029	0.0252	0.0617	0.0305	0.0377
z	0.0018	0.0313	0.0604	0.0361	0.0538
ϕ	0.0139	0.0375	0.0301	0.0214	0.0181
θ	0.0090	0.0409	0.0217	0.0183	0.0298
ψ	0.0007	0.0016	0.0021	0.0038	0.0032

Table 3. IAU and IADU performance indexes.

Control plan	Performance indexes					
	IAU			IADU		
	u_2	u_3	u_4	u_2	u_3	u_4
Scenario 1						
Proposed NDOB-AFNTSM	0.6658	0.5053	0.5750	17.2129	17.7586	8.2152
NTSMC	1.1162	1.2432	2.6039	155.135	167.748	519.772
TSMC	6.734	6.209	10.751	1134.689	1165.825	1981.376
FGTSMC	1.6152	1.7197	1.3105	23.7393	29.8791	0.6249
Scenario 2						
Proposed NDOB-AFNTSM	0.8076	0.9296	0.5204	24.0321	26.2360	19.9989
NTSMC	2.0729	2.1890	5.0698	272.1119	272.0264	830.2334
TSMC	11.0475	11.7287	19.0282	2136.141	2066.514	1477.515
FGTSMC	0.9425	1.0859	0.9727	44.3854	47.3340	0.5544

Declaration of conflicting interests

The author(s) declared no potential conflicts of interest with respect to the research, authorship, and/or publication of this article.

Funding

The author(s) disclosed receipt of the following financial support for the research, authorship, and/or publication of this article: This work is supported by the National Natural Science Foundation of China (62003103).

ORCID iD

Yan Jiang  <https://orcid.org/0000-0001-6031-8457>

References

1. Al-Ali I, Zweiri Y, AMoosa N, et al. State of the art in tiltquadrotors, modelling, control and fault recovery. *Proc IMechE, Part C: J Mechanical Engineering Science* 2020; 234(2): 474–486.
2. Shihavuddin ASM, Chen X, Fedorov V, et al. Wind turbine surface damage detection by deep learning aided drone inspection analysis. *Energies* 2019; 12(4): 676.
3. Mofid O and Mobayen S. Adaptive sliding mode control for finite-time stability of quad-rotor UAVs with parametric uncertainties. *ISA Trans* 2018; 72: 1–14.
4. Salih A, Moghavvemi M, Mohamed H, et al. Modelling and PID controller design for a quadrotor unmanned air vehicle. In: *2010 IEEE international conference on automation, quality and testing, robotics (AQTR)*, volume 1, 2010, pp.1–5. New York: IEEE
5. Castillo P, Lozano R and Dzul A. Stabilization of a mini rotorcraft with four rotors. *IEEE Control Syst* 2005; 25(6): 45–55.
6. Aboudonia A, El-Badawy A and Rashad R. Active anti-disturbance control of a quadrotor unmanned aerial vehicle using the command-filtering backstepping approach. *Nonlinear Dyn* 2017; 90(1): 581–597.
7. Shao X, Liu J and Wang H. Robust back-stepping output feedback trajectory tracking for quadrotors via extended state observer and sigmoid tracking differentiator. *Mech Syst Signal Process* 2018; 104: 631–647.
8. Yang H, Cheng L, Xia Y, et al. Active disturbance rejection attitude control for a dual closed-loop quadrotor under gust wind. *IEEE Trans Control Syst Technol* 2018; 26(4): 1400–1405.
9. Zhao W and Go TH. Quadcopter formation flight control combining MPC and robust feedback linearization. *J Franklin Inst* 2014; 351(3): 1335–1355.
10. Bansal S, Akametalu A, Jiang F, et al. Learning quadrotor dynamics using neural network for flight control. In: *IEEE 55th conference on decision and control (CDC)*, 2016, pp.4653–4660. New York: IEEE.
11. Li S, Wang Y, Tan J, et al. Adaptive RBFNNs/integral sliding mode control for a quadrotor aircraft. *Neurocomputing* 2016; 216: 126–134.
12. Xiong JJ and Zhang GB. Global fast dynamic terminal sliding mode control for a quadrotor UAV. *ISA Trans* 2017; 66: 233–240.
13. Utkin V. Variable structure systems with sliding modes. *IEEE Trans Automat Contr* 1977; 22(2): 212–222.
14. Yu S, Yu X, Shirinzadeh B, et al. Continuous finite-time control for robotic manipulators with terminal sliding mode. *Automatica* 2005; 41(11): 1957–1964.
15. Feng Y, Yu X and Man Z. Non-singular terminal sliding mode control of rigid manipulators. *Automatica* 2002; 38(12): 2159–2167.
16. Kahouadji M, Mokhtari MR, Choukchou-Braham A, et al. Real-time attitude control of 3 DOF quadrotor UAV using modified super twisting algorithm. *J Franklin Inst* 2020; 357(5): 2681–2695.
17. Razmi H and Afshinifar S. Neural network-based adaptive sliding mode control design for position and attitude control of a quadrotor UAV. *Aerosp Sci Technol* 2019; 91: 12–27.
18. Vahdanipour M and Khodabandeh M. Adaptive fractional order sliding mode control for a quadrotor with a varying load. *Aerosp Sci Technol* 2019; 86: 737–747.
19. Hua C, Chen J and Guan X. Fractional-order sliding mode control of uncertain QUAVs with time-varying state constraints. *Nonlinear Dyn* 2019; 95(2): 1347–1360.
20. Wang J, Wang P and Ma X. Adaptive event-triggered control for quadrotor aircraft with output constraints. *Aerosp Sci Technol* 2020; 105: 105935.
21. Mechali O, Xu L, Huang Y, et al. Observer-based fixed-time continuous nonsingular terminal sliding mode control of quadrotor aircraft under uncertainties and disturbances for robust trajectory tracking: theory and experiment. *Control Eng Pract* 2021; 111: 104806.
22. Ullah N, Mehmood Y, Aslam J, et al. Fractional order adaptive robust formation control of multiple quad-rotor UAVs with parametric uncertainties and wind disturbances. *Chin J Aeronaut* 2022; 35(8): 204–220.
23. Zhao L, Dai L, Xia Y, et al. Attitude control for quadrotors subjected to wind disturbances via active disturbance rejection control and integral sliding mode control. *Mech Syst Signal Process* 2019; 129: 531–545.
24. Akhil M, Anand M, Sreekumar A, et al. Simulation of the mathematical model of a quadrotor control system using matlab simulink. *Appl Mech Mater* 2012; 110: 2577–2584.
25. Eltayeb A, Rahmat M, Eltoum M, et al. Adaptive fuzzy gain scheduling sliding mode control for quadrotor UAV systems. In: *8th international conference on modeling simulation and applied optimization (ICMSAO)*, 2019, pp.1–5. New York: IEEE.
26. Yang Y and Yan Y. Attitude regulation for unmanned quadrotors using adaptive fuzzy gain-scheduling sliding mode control. *Aerosp Sci Technol* 2016; 54: 208–217.
27. Labbadi M and Cherkaoui M. Robust adaptive non-singular fast terminal sliding-mode tracking control for an uncertain quadrotor UAV subjected to disturbances. *ISA Trans* 2020; 99: 290–304.
28. Wang H, Ye X, Tian Y, et al. Model-free-based terminal SMC of quadrotor attitude and position. *IEEE Trans Aerosp Electron Syst* 2016; 52(5): 2519–2528.
29. Tripathi VK, Yogi SC, Kamath AK, et al. A disturbance observer-based intelligent finite-time sliding mode flight controller design for an autonomous quadrotor. *IEEE Syst J* 2022; 16(1): 1649–1660.
30. Amin RU, Inayat I and Ai Jun L. Finite time position and heading tracking control of coaxial octocopter based on extended inverse multi-quadratic radial basis

- function network and external disturbance observer. *J Franklin Inst* 2019; 356(8): 4240–4269.
- 31. Man Z and Yu X. Adaptive terminal sliding mode tracking control for rigid robotic manipulators with uncertain dynamics. *JSME Int J C* 1997; 40(3): 493–502.
 - 32. Song Y, Huang X and Wen C. Tracking control for a class of unknown nonsquare MIMO nonaffine systems: A deep-rooted information based robust adaptive approach. *IEEE Trans Automat Contr* 2016; 61(10): 3227–3233.
 - 33. Shao K, Zheng J, Huang K, et al. Finite-time control of a linear motor positioner using adaptive recursive terminal sliding mode. *IEEE Trans Ind Electron* 2020; 67(8): 6659–6668.
 - 34. Lian S, Meng W, Lin Z, et al. Adaptive attitude control of a quadrotor using fast nonsingular terminal sliding mode. *IEEE Trans Ind Electron* 2021; 69(2): 1597–1607.
 - 35. Xia Y, Xu K, Li Y, et al. Improved line-of-sight trajectory tracking control of under-actuated AUV subjects to ocean currents and input saturation. *Ocean Eng* 2019; 174: 14–30.
 - 36. Ho CM, Tran DT and Ahn KK. Adaptive sliding mode control based nonlinear disturbance observer for active suspension with pneumatic spring. *J Sound Vib* 2021; 509: 116241.
 - 37. Chen WH. Nonlinear disturbance observer-enhanced dynamic inversion control of missiles. *J Guid Control Dyn* 2003; 26(1): 161–166.
 - 38. Ioannou P and Sun J. *Robust adaptive control*. Hoboken, NJ: PTR Prentice-Hall, 1996.
 - 39. Gao W and Hung J. Variable structure control of nonlinear systems: a new approach. *IEEE Trans Ind Electron* 1993; 40(1): 45–55.
 - 40. Napole C, Derbeli M and Barambones O. A global integral terminal sliding mode control based on a novel reaching law for a proton exchange membrane fuel cell system. *Appl Energy* 2021; 301: 117473.